RESEARCH ARTICLE

Experimental Study on the Effect of Extreme Waves on a LNG Carrier

Marco Klein[1,2], Shan Wang[3], Günther Clauss[4] and C. Guedes Soares[3]

Abstract

This paper presents a comprehensive experimental study on the effect of extreme waves on a LNG carrier. The LNG carrier model was equipped with a variety of sensors to measure motions, green water height on deck as well as local and global loads. Experiments in transient wave packets provided the general performance in waves in terms of response amplitude operators and were accompanied by tests in regular waves with two different wave steepness. These tests allowed detailed insights into the nonlinear behavior of the vertical wave bending moment in steep waves showing that green water on deck can contribute to a decrease of vertical wave bending moment. Afterwards, systematic model tests in irregular waves were performed to provide the basis for statistical analysis. It is shown that the generalized extreme value distribution model is suitable for the estimation of the extreme peak values of motions and loads. Finally, model tests in tailored extreme wave sequences were conducted comparing the results with the statistical analysis. For this purpose, analytical breather solutions of the nonlinear Schrödinger equation were applied to generate tailored extreme waves of certain critical wave lengths in terms of ship response. Besides these design extreme waves, the LGN carrier was also investigated in the model scale reproduction of the real-world Draupner wave. By comparing the motions, vertical wave bending moment, green water column and slamming pressures it is concluded that the breather solutions are a powerful and efficient tool for the generation of design extreme waves of certain critical wave lengths for wave/structure investigations on different subjects.

Keywords Extreme wave events; Wave-structure interaction; Draupner wave; Breather solutions

Article Highlights

- A comprehensive experimental study on the impact of extreme waves on a LNG carrier is presented in terms of the ship motions, vertical bending moments (VBM), green water heights, and slamming loads.
- The model tests in regular waves show that the green water on deck causes the decrease of VBM for wave lengthip length = 1.1.
- The nonlinear behavior in higher, steeper waves can be investigated systematically in regular waves.
- The statistical analysis for irregular wave tests shows that the GEV distribution model is suitable for the estimation of the extreme peak values of motions and loads.
- The statistical analysis for Draupner extreme wave tests shows that the analytical breather solutions are good alternatives for the real work freak waves in the investigation of ship motions and loads.

✉ Marco Klein
  marco.klein@dlr.de

1   German Aerospace Center (DLR), Institute of Maritime Energy Systems, Max-Planck-Straße 2, Geesthacht 21502, Germany

2   Hamburg University of Technology, Offshore Dynamics Group, Schloßmühlendamm 30, Hamburg 21073, Germany

4   Centre for Marine Technology and Ocean Engineering (CENTEC), Instituto Superior Técnico, Universidade de Lisboa, Avenida Rovisco Pais, Lisboa 1049-001, Portugal

5   Technische Universität Berlin, Ocean Engineering Division, Salzufer 17-19, Berlin 10587, Germany

1 Introduction

Extreme waves are characterized by significantly high wave amplitudes and short time duration, leading to large motions and loads on marine structures. The risk for ships encountering extreme sea states has been confirmed by the reported accidents in the last years with increasing frequency. A general overview of real sea extreme wave registrations and reported accidents can be found in Kharif et al. (2008). The occurrence of hurricanes in the Gulf of Mexico has confirmed further that extreme sea states can be dangerous for marine structures. It is likely that the significance of severe sea state conditions for ship traffic will even grow in the future because of the expected increase in frequency and severity of extreme weather events associated with global warming.

Earlier investigations indicate that ship response may significantly increase in extraordinarily steep and/or large (extreme) waves and a proper prediction of responses due to extreme waves is important for ship safety in the extreme sea. There are only a few reported experimental studies with the ship responses in realistic extreme wave conditions. Stansberg and Karlsen (2001) have performed model tests with an FPSO in steep random waves showing that

the ship motions are an important parameter besides the encountering wave profile and indicating that the relative short and steep waves are more critical than longer waves, due to the phase lag of the pitch motion, in particular in combination with large pitch amplitudes. The vertical bending moment (VBM) on FPSO due to extreme wave have been investigated by Clauss et al. (2004) and Guedes Soares et al. (2006) by comparing numerical simulations and model tests. The variation of the maximum bending moment with the position in space where the extreme wave was created has been investigated and found to have a small influence. Drummen et al. (2009) have compared the experimental and numerical responses of a modern container ship with a large bow flare in severe head seas. Denchfield et al. (2009) have calculated the symmetric motions and global wave-induced loads for a Leander class frigate in head irregular and extreme waves using a two-dimensional hydroelastic method comparing the rigid body motions with experiments. The investigation of Fonseca and Guedes Soares (2002) and Clauss et al. (2010) have shown for different types of ships that the geometry of the bow flare in combination with the wave steepness influence the global loads significantly, in particular the sagging loads. A segmented model of a RoRo vessel with a large bow flare has been tested in regular and two real-sea waves by Clauss et al. (2010), showing that critical loads and motions depend most notably on combinations of wave height, wave group sequences, crest steepness, encountering speed and the ships target position. Even small wave heights with unfavorable wave lengths can cause a critical situation.

Slamming and green water phenomenon often happens for various vessels in extreme seas. Clauss et al. (2012) have presented the systematic experimental study of an LNG carrier and a chemical tanker in high, steep waves in the seakeeping basin using breather solutions, showing that the impact of a extreme wave is severe and dangerous resulting in large loads and huge amount of green water on deck. Slamming impacts on a chemical tanker subjected to extreme waves have been investigated experimentally and numerically in Wang and Guedes Soares (2016a, b). Slamming occurrence on the chemical tanker advancing in extreme waves modelled with the nonlinear Schrödinger equation has been studied by Wang et al. (2016). Wang et al. (2020) has studied the hydroelastic response of a river-sea-going containership. Green water loading on the hatch covers of bulk carriers in extreme weather conditions has been estimated by Vassalos et al. (2003) using empirical equations.

In addition to experimental analysis, numerical solutions based on potential flow are more frequently used. The time domain strip theory method (Fonseca and Guedes Soares 1998a, b) has been validated for predictions of responses to abnormal waves (Guedes Soares et al. 2008; Fonseca et al. 2010), showing that the code overestimates the sagging moment peaks in very large and steep waves (Rajendran

et al. 2011, 2012). The code has been extended to include the body nonlinearities in the radiation and diffraction forces and then applied for predicting the vertical motions and loads for a cruise ship subject to large amplitude waves (Rajendran et al. 2015; Rajendran and Guedes Soares 2016). This time domain code has been coupled with a FE model in Rajendran et al. (2016) for investigating the flexible vertical response of container ships in high seas. Good results are obtained for low Froude numbers and head waves to strip theory codes; however, the accuracy decreases for other headings and higher speeds.

The 3D Boundary Element Method (BEM) uses either a Wave Green's Function (WGF) or a Rankine Source (RS) as a source potential to satisfy boundary conditions. Yasukawa (2002) have applied the 3D Rankine Panel method in the time domain to calculate ship motions and local pressure of several container ships with a large flare comparing the results with model test and strip theory. Zakaria (2009) has used the linear 3D Panel method to predict the relative wave height of container ships in extreme seas. Guo et al. (2013) have studied ship response statistics in extreme seas using WASIM. Datta and Guedes Soares (2020) have analysed the hydroelastic response of a container vessel using a coupled BEM-FEM method.

The application of RANS solver in simulating ship responses in waves has been intensively investigated in recent years (Oberhagemann et al. 2012; Simonsen et al. 2013; Tezdogan et al. 2015; Jiao et al. 2021a, b). Most of them have been validated against experiments and show very promising results. However, the numerical errors due to uncertainties are still a concern, and it is difficult to perform CFD simulations on many severe sea states due to high computational costs.

The number of model tests investigating ship responses in extreme waves is still limited today while the existing numerical codes predicting ship behavior in these waves still need to be improved. To ensure the accuracy of numerical solutions, uncertainty quantification has been emphasized in recent years. The investigation of numerical errors due to discretization of CFD solvers can be found in Huang et al. (2022) for wave loads and hydroelastic responses of a container ship, and in Wang et al. (2021) for slamming load predictions.

The results of a benchmark study, organised by the ISSC-ITTC Joint Committee, on global linear wave loads on a container ship with forward speed has been presented in Parunov et al. (2022). The objective of the study was to assess the uncertainty in linear transfer functions due to different seakeeping codes and consequences on long-term extreme vertical wave bending moments. For this study, the well documented Flokstra's container ship with accessible experimental data has been selected. The study has confirmed that large differences can be found between methods based on the same mathematical model and recommended the initiation of benchmark studies with different ship types to

provide the basis for the quantification of uncertainties.

Within the EU project EXTREME SEAS, an extensive experimental study of the ship motions and wave-induced local and global loads of an LNG carrier in extreme seas has been conducted, however, only part of the experimental data have been made accessible for the public. To provide a general overview on the test setup, the experimental program and main findings as database for the benchmark study, this paper presents a comprehensive analysis of the impact of extreme waves on an LNG carrier, including the ship motions, VBM amidships, slamming, and green water impact loads of the model due to regular, irregular, and extreme waves. Main findings regarding motions and loads on the ship from previous studies will be summarized as well.

2 Model tests

The model tests were conducted in the seakeeping basin of the Ocean Engineering Division of the Technical University Berlin. The basin is 110 m long, with a measuring range of 90 m, the width is 8 m and the water depth is 1 m. On one side, an electrically driven wave generator is installed which can be used in piston-type as well as flap-type mode. The wave generator is fully computer controlled and a software is implemented which enables the generation of transient wave packages, deterministic irregular sea states with defined characteristics as well as tailored critical wave sequences. On the opposite side, a wave-damping slope is installed to suppress wave reflections.

2.1 LNG carrier model

The LNGC model was made of fibreglass reinforced plastic (GRP) in model scale 1 : 70. The main dimensions are given in Table 1. An impression of the LNGC model is presented in Figure 1(a). The origin for all subsequent position specifications is shown in Figure 1(b). A detailed mass distribution of the investigated LNGC model is given in Table A1 in Appendix A.

2.2 Model equipment

The model was equipped with several different sensors to measure global ship motions, global and local loads and

Table 1 Main dimensions of the LNGC

Parameters	Full scale	Model scale
Length over all (L_{OA})	197.13 m	2.816 m
Length between perpendicular (L_{pp})	186.90 m	2.670 m
Breadth	30.38 m	0.434 m
Depth (moulded bulwark in the model)	18.20 m	0.268 m
Draught	8.40 m	0.120 m
Displacement	35 674.8 t	103.831 kg

the wave profile at the bow on the weather deck. Following, each individual measuring equipment is introduced in detail.
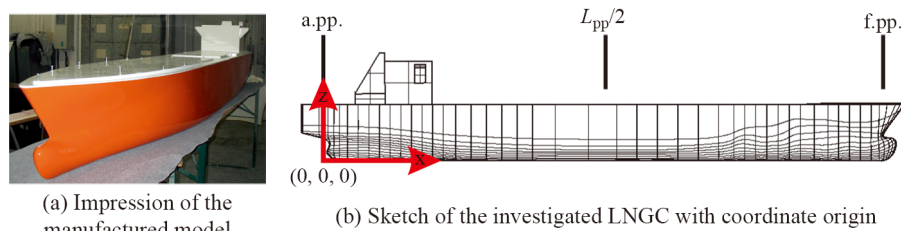
2.2.1 Pressure transducers

The model was instrumented with pressure transducers at different positions on the hull: on the bow, on deck at the forecastle area and on the keel near the bow and at the stern. Figure 2 presents sketches of the pressure transducer locations at bow (Figure 2(a)) and stern (Figure 2(c)) as well as shows the installion of the pressure transducers at bow exemplary (Figure 2(b)).
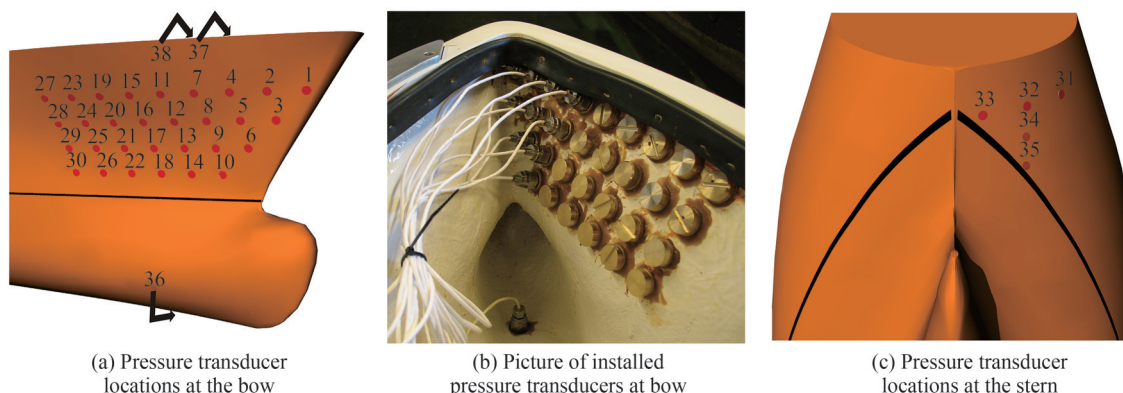
The overall focus of the experiments lied on the pressure loads on the bow due to steep large waves. Therefore, a large area at the bow of the vessel was instrumented with pressure transducers to obtain conclusions regarding the local pressure distribution on the bow and the associated global effects on the vbm (cf. Figure 2(a)). A detailed description of the position of the transducers as well as its measuring characteristics and uncertainties can be found in Appendix B.
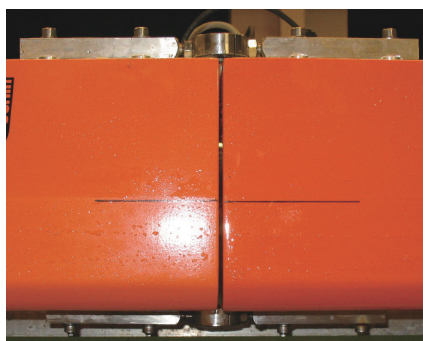
2.2.2 Force transducers

For the determination of the global loads, particularly the vertical wave bending moment, the ship model was divided into two segments which were connected with three force transducers. Two were mounted on deck, one on each side, the third one was mounted underneath the keel (cf. Figure 3). The force transducers registered the longitudinal forces during the model tests. Based on the measured forces and the given geometrical arrangement of the three force transducers, the resulting vertical wave bending moment and the longitudinal forces were obtained. The strain gauges featured a nominal load of 200 kg and a protection class of IP68 (100 h at 1 m water column).

(a) Impression of the manufactured model

(b) Sketch of the investigated LNGC with coordinate origin

Figure 1   Sketch of the investigated LNGC and the manufactured model

(a) Pressure transducer
locations at the bow

(b) Picture of installed
pressure transducers at bow

(c) Pressure transducer
locations at the stern

Figure 2   Overview on the pressure transducer locations

Figure 3   Sideview of the mounted force transducers

2.2.3 Green water and relative wave gauges

In addition to the two pressure sensors (No. 37 & No. 38) mounted on deck, two green water gauges (absolute, measurable green water height on deck is 0.185 m and 0.125 m) were installed at the same longitudinal positions. The positions and dimensions are illustrated in Figure 4. Furthermore, a relative wave gauge ($h_{relative}$=0.75 m) was installed at the bow at the forward perpendicular.

2.3 Test set-up

The test set-up included the suspension system to hold the model in position during the tests, the tracking system to measure the absolute motions as well as the wave gauges to measure the encountering waves.
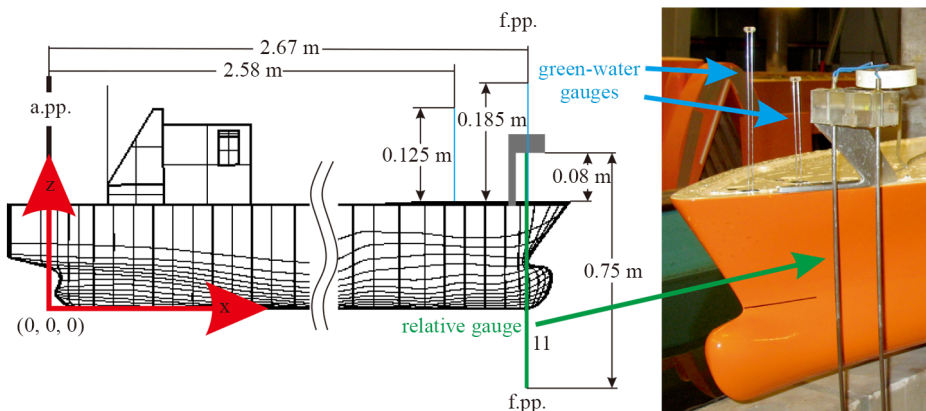
2.3.1 Suspension system

During the investigations, the model was fixed with an elastic suspension system using a triangular towing arrangement pulling the model without inducing a moment (cf. Figure 5(a)). The longitudinal motions were restricted by a spring in front of and a counter weight behind the model. With this arrangement, heave and pitch motions as well as the measured forces and moments remained unrestrained.

To evaluate the influence on the vbm, investigations were made in steep, regular waves with and without suspension system. Figure 5(b) compares the vbm at waterline level with and without suspension system. The investigation revealed that the influence is less than 2% and can be neglected.

2.3.2 Absolute motions

The ship motions were recorded by an optical tracking system. The tracking system consists of a seven by ten meter frame that carries five infrared cameras which were shifted parallel to the moving ship model. The system enables high precision, contact-free motion tracking over large distances by following the trajectories of infrared light emitting diodes mounted on the ship model.

Figure 4   Positions and dimensions of the relative wave gauge and the green water gauges

(a) Top view on
the test set-up

(b) Comparison between vbm at waterline level measured with
and without suspension system
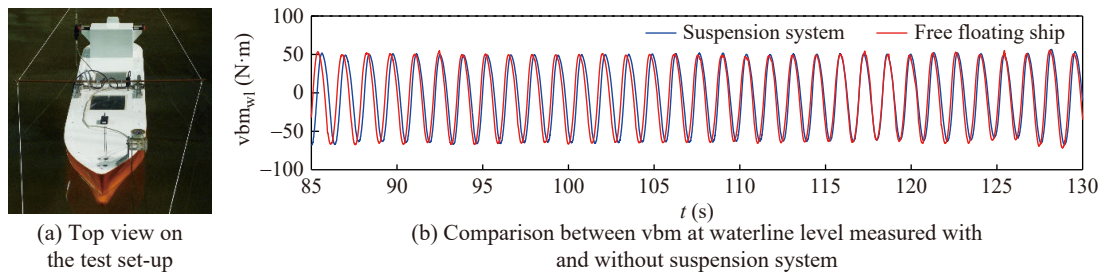
Figure 5   Test set-up and evaluation of the suspension system

2.3.3 Wave gauge positions

The number of wave probes as well as they positions were varying according to the objective of the test campaigns. Altogether, the LNGC was investigated at stationary conditions and at forward speed. At stationary conditions, one objective lied on a detailed detection of the wave evolution along the ship, particularly at the forward perpendicular. Figure 6 shows the sketch of the wave gauge positions for the model test at stationary conditions. The investigations were performed at a target location at 45.9 m, starting at the idle state of the wave board. Target point was the forward perpendicular of the LNGC. A total amount of ten wave gauges were installed about the target location. The first one is 6 m in front of it at x_{t1}=39.9 m. A cluster of seven gauges, separated in 0.1 m intervals, was arranged around the target location to investigate the spatial evolution of the waves at the bow. Furthermore two gauges, one at each position, were installed amidships and at the aft perpendicular. For the cruising ship, this set-up was reduced to three wave gauges-one 6 m in front of the forward perpendicular (gauge No. 1 in Figure 6), one at forward perpendicular (gauge No. 5 in Figure 6) and one at amidships (gauge No. 9 in Figure 6) regarding the idle state of the model.

## 3 Experimental program and results

The experimental program included investigations in frequency and time domain. One objective of the model tests was the determination of the response in terms of transfer functions. Therefore the model was investigated in transient wave packages to obtain the Response Amplitude Operator (RAO) and the results were evaluated with tests in regular waves. Furthermore the model was investigated in irregular sea states, critical wave sequences, and real world freak wave reproductions as well as in breather-type freak waves. In the following subsections, the different parts of the experimental program are presented.

3.1 Transient wave packet

A powerful and efficient tool for the evaluation of the sea state behavior of ships and offshore structures is the transient wave packet technique which enables the determination of the RAO efficiently in one test run (e.g., Clauss and Küuhnlein 1995, 1997; Clauss and Steinhagen 1999; Kühnlein et al. 2002; Clauss et al. 2010; Hennig 2005; Clauss et al. 2014; Klein et al. 2021). TWP's depict synthesized task-related wave spectra with tailored phase distribution. The phase distribution is adjusted in such a way that all components of the wave spectrum are in-phase superimposed at the concentration point yielding a single wave peak. The shape and width of the spectrum can be adapted to the relevant frequency range of interest.

Figure 7 presents the RAO's determined by the TWP technique. For comparative and evaluation purposes, the experimental results (blue curves) are compared with numerical results (red curves) obtained by the well established frequency domain analysis program WAMIT (Wave Analysis at Massachusetts Institute of Technology). WAMIT is a radiation/diffraction program for the evaluation of wave-structure interaction at zero speed in frequency domain (Newman 2018; WAMIT 1994; Lee 1995) being a widely
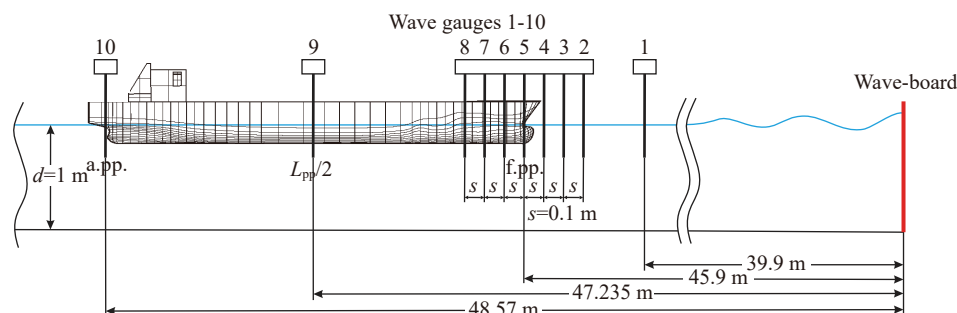
Figure 6   Sketch of the wave gauge positions

accepted, validated numerical tool for hydrodynamic analysis and proven to be suitable for a multitude of applications. Figure 7(a) presents the result for heave motion, Figure 7(b) for pitch motion and Figure 7(c) for the vbm. The good agreement between the experimental and numerical results is evident at first glance.

3.2 High and steep regular waves

The investigated discrete regular wave lengths (L_w) were chosen in order to cover the complete range of interest in frequency domain-from L_w/L_{pp}=0.6 to L_w/L_{pp}=2.2. With regard to the influence of the wave steepness on the vbm, the test program was divided into two parts. Each part comprised the same wave lengths with varying wave steepness. The wave height and steepness was selected in such a way to obtain wave profiles with different crest/trough asymmetries and to evaluate the influence of different wave profiles (asymmetries) on the vbm.

Figure 8 illustrates the regions of validity of various gravity water wave theories with regard to the wave profile. The relative water depth is plotted on the abscissa and the relative wave height on the ordinate. It is shown that for small amplitude waves, the linear wave theory can be applied, whereas for increasing wave heights (and hence increasing crest/trough asymmetries) the Stokes II and Stokes III theories become valid (the relative water depth of the investigated wave lengths is between $0.02 \leqslant d/(g \cdot T^2) \leqslant 0.1$ (cf. Figure 8).

The first part of the experimental program included regular waves with moderate amplitudes. The relative wave heights of the investigated waves were between $0.002 \leqslant H/(g \cdot T^2) \leqslant 0.004$ - where the wave profile was within the Stokes II domain (cf. Figure 8 - red dots). During the second part of the experimental program, the same (regular) wave lengths were generated with increased relative wave heights and thus the relative wave heights were between $0.01 \leqslant H/(g \cdot T^2) \leqslant 0.012$ - where the wave profile was within the Stokes III domain (cf. Figure 8 - blue dots).

Figure 9 presents the results of the model tests in regular waves-the respective RAOs (|sagging moment| + hogging moment-red dashed curves) are compared to the RAO (black curves) determined by the transient wave packet

technique. The sagging (red crosses) and hogging moments (red circles) are additionally registered to evaluate the asymmetry of the measured bending moment compared to the wave steepness. Figure 9(a) shows the result for wave profiles in the Stokes II domain (WH2) and Figure 9(b) for wave profiles in the Stokes III domain (WH3).

The result of the RAO's determined in regular waves (|sagging moment| + hogging moment - red dashed curves) and in the transient wave packet (black curves) are in good agreement. With regard to the asymmetry of the hogging and sagging moments, it is clearly identifiable that the asymmetry between sagging and hogging increases with increasing wave height which is in accordance to previous investigations (Watanabe et al. 1989; Guedes Soares and Schellin 1998; Fonseca and Guedes Soares 2005; Clauss and Klein 2016). The trend of the vbm, in particular regarding the results in the WH3 regular waves, shows a special feature - a hollow at the interval where the maximum of the RAO would be expected for the LNG Carrier. This does not denote that the vbm shrunk but that the vbm shrunk proportionally to the wave height. It is noticeable that this occurs around $L_w/L_{pp} = 1.1$ and can be explained with the effect of green water on deck.

Figure 10 presents the green water column height on deck of the LNGC for the different wave length. The installed green water sensors are capable to detect continuous water volumes, but the green water on deck behaves like a spilling breaking wave with white cap. This results in a scatter of the detected green water column heights (indicated in Figure 10 via the associated variance). However, it is clear identifiable that the interval of the highest green water columns is within the observed hollow interval regarding the vbm. This shows that the vbm shrunk proportionally to the wave height due to the fact that some of the energy of the increased wave crest spills over the deck in terms of green water instead of acting on the bow resulting in a smaller vbm to wave height ratio. Furthermore, additional effects due to the influence of the shipping of water on deck have to be taken into account such as affected ship motions (Fonseca and Guedes Soares 2005) as well as a counteracting moment due to the green water mass on deck (Rajendran et al. 2011; Clauss and Klein 2016).
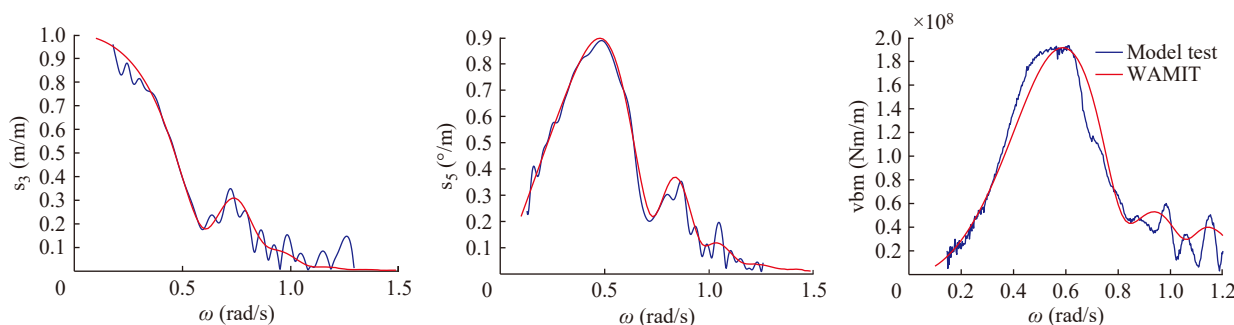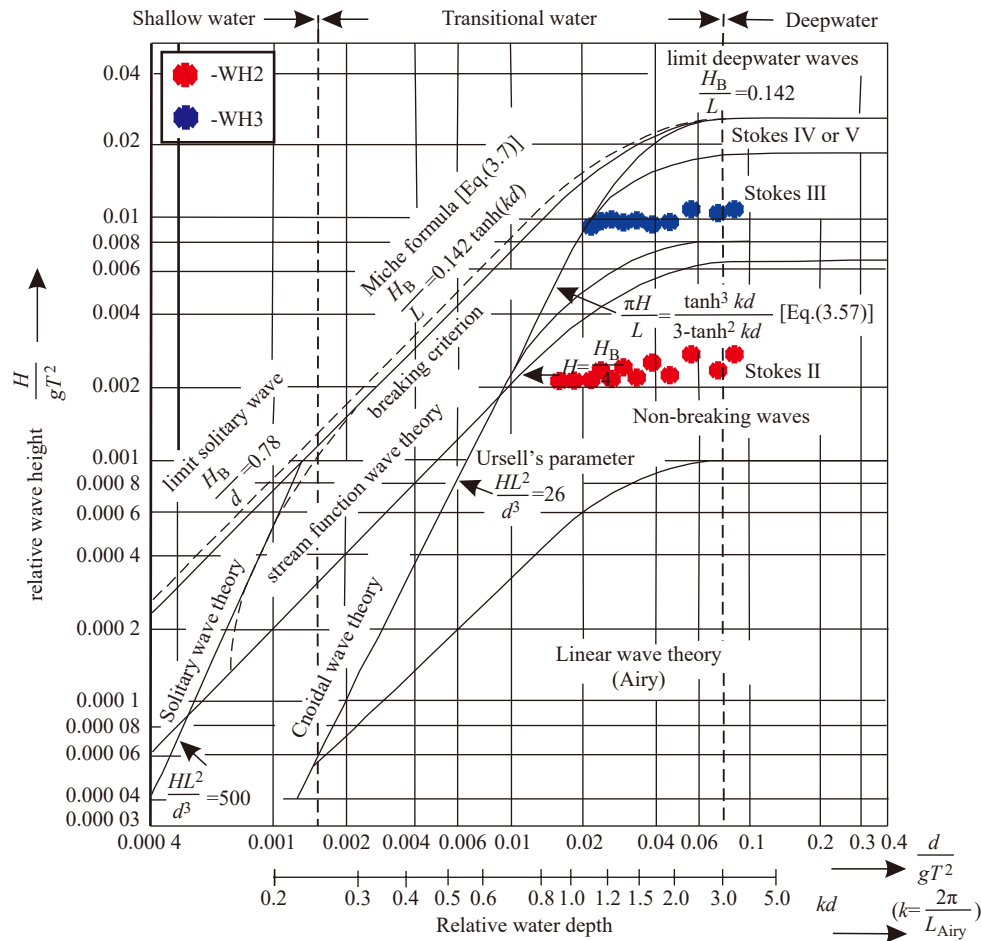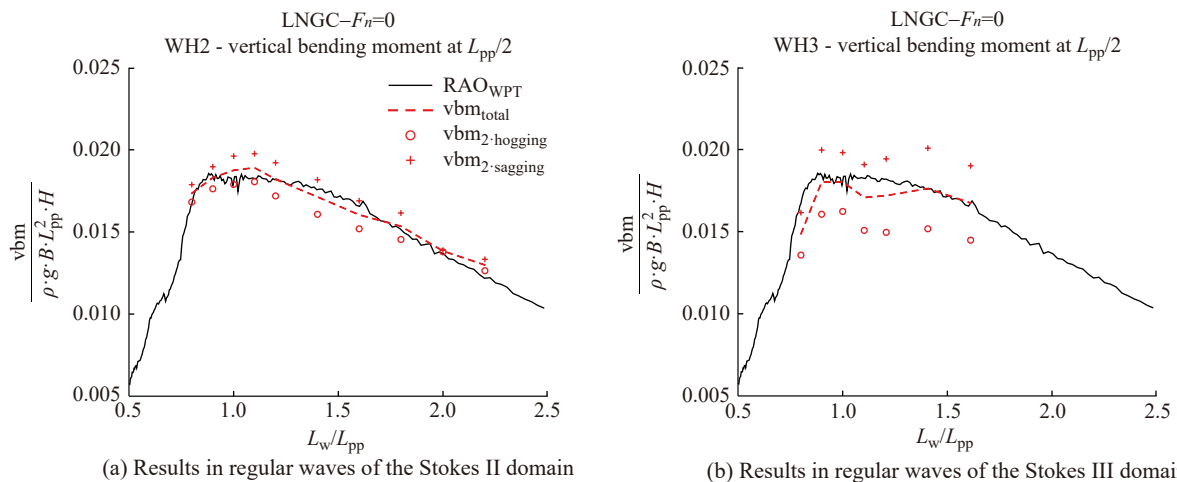

Figure 7 Comparison of measured (blue curves) and calculated RAOs (red curves) for the LNGC

Figure 8 Breaking wave height and regions of validity of various gravity water waves' theories (Clauss et al. 1992)


Figure 9 Comparison of the RAO for the vbm at $L_{pp}/2$ determined with the transient wave package technique (black curves) and the results in regular waves (red dashed curves) for the LNG Carrier. The sagging (red crosses) and hogging moments (red circles) are additionally registered

3.3 Irregular sea states with random phases

Several irregular sea states were investigated representing design storms according to existing probabilistic methods. The investigated characteristic sea state parameters T_p, H_s and γ are given in Table C3 in Appendix C. These sea states, each about 30 min real time, were generated in groups of up to six sea state sequences (phase seeds) per characteristic sea state parameter set for long term statistical analysis and each row presents one set of the characteristic irregu-

LNGC–Fn=0
WH3-green water column at forward perpendicular
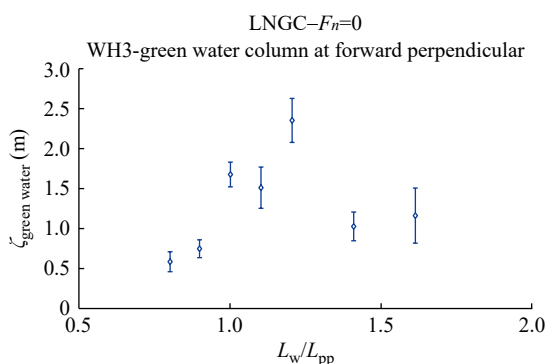
Figure 10 Green water column height on deck of the LNGC at the forward perpendicular

lar sea state parameters. The phases were randomly generated and differ within each set of parameters but are constantly plugged for each set. For example, parameter set No. 1 (see Table C3), phase seed #1 had another random phase distribution than phase seed #2, #3 and so on of the same set, but the same phase seed like set No. 2, phase seed #1, set No. 3, phase seed #1 and so on. Altogether, 45 irregular sea states for test runs at stationary conditions (Fn=0) as well as at forward speed (Fn=0.07).

In the following, the experimental results for sea state IRREGULAR20 (cf. Table C3) at Fn=0 are presented. The focus lies on the statistical analysis of the excceedance probability of the peaks of global motions and loads. For comparative purposes, the experimental results are compared to numerical simulations. Therefore, a strip theory based partially nonlinear time domain code was applied (Rajendran et al. 2015).

Figure 11 compares the time series of the numerical solution and the measured incident waves, heave and pitch motions, and the vbm at amidships (Fn=0 and sea state IRREGULAR20). The wave profile recorded at amidships (cf. No. 9 in Figure 6) were directly converted to the input data for the numerical simulation. As seen in Figure 11(a), the numerical wave sequence is in perfectly good agreement with the measurements. However, as the wave profile in space domain is based on linear transformation of the registration amidships, the wave profile along the ship in space domain will differ from the experiments. In addition and in contrast to the experiments, the ship's position in space is fixed. Reading the motions (Figure 11(b) and 11(c)) and loads (Figure 11(d)), the agreement between numerical and experimental values are satisfactory in general, though the numerical method overpredicts the peaks slightly.

Figure 12 shows the comparison of the exceedance probability of the peaks for IRREGULAR20 phase seed #1.

(a) Wave elevation at amidships

(b) Heave motion

(c) Pitch motion
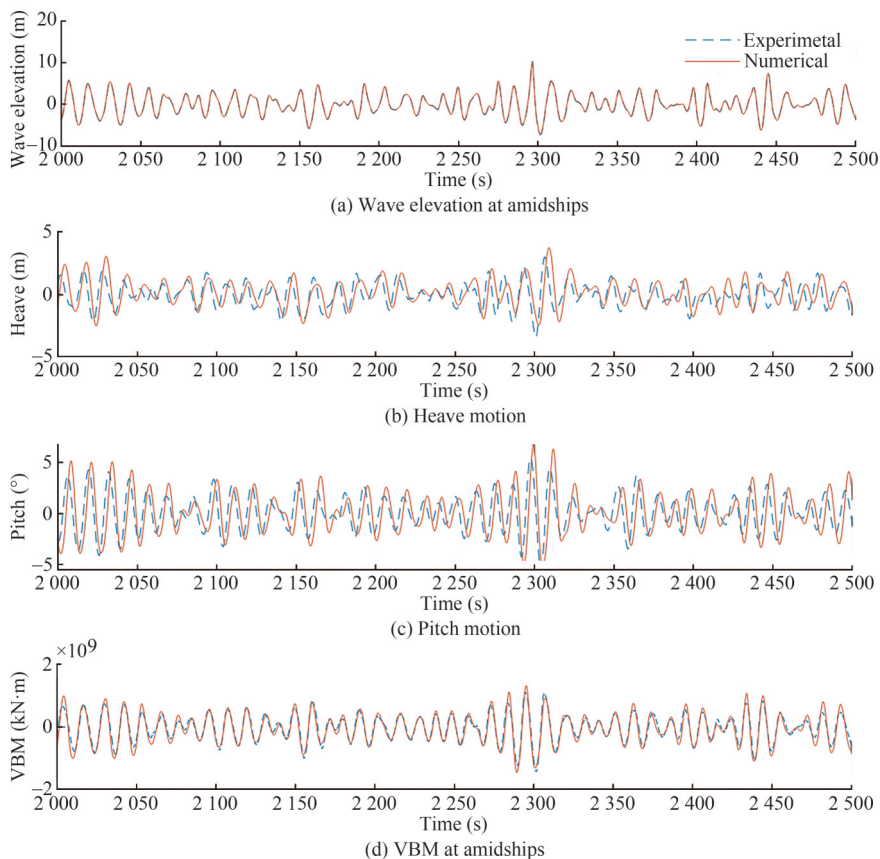
(d) VBM at amidships

Figure 11 Comparison of the numerical prediction of the time series of the wave surface elevation at amidships, heave, pitch and vbm with experiments in the sea state IRREGULAR20 phase seed #1

For the experimental data, negative heave peaks are larger than the positive ones for the measured responses except the tails, while the positive pitch peaks are higher than the negative ones. The numerical heave peaks follow similar trends for all the results; however, they are all higher than the experimental peaks at the same probability.

Taking all five phase seeds of IRREGULAR20 into account gives the exceedance probability of the peaks presented in Figure 13. For the heave motion, the positive and negative values are very close when the exceedance probability is high, but the difference becomes larger when the exceedance probability is getting smaller. A similar observation is found for pitch motion. Comparing the values from the five repeated tests, the exceedance probabilities for the peaks agree quite well for small values, but more deviations are found for larger values. It is expected that the uncertainty in extreme value is higher.

To study the peak values of the ship motions and loads subjected to extreme waves, the generalized extreme value (GEV) distribution model was applied on the experimental data. The statistical analysis showed that the GEV distribution model is suitable for the estimation of the extreme peak values. Figure 14 presents diagnostic plots of goodness of fit for generalized extreme value distribution of the peak values from the experiments. The random uncertainties of the experimental data for the motions and vbm are

small (below 3.2 %) for the Fn=0 case. For the case with a forward speed (Fn=0.07), all uncertainties are below 2.2% (cf. Wang and Guedes Soares 2022b). Compared with the random uncertainty of the slamming peaks, the experimental errors of motions and vbm are quite small. A detailed analysis and discussion can be found in Wang and Guedes Soares (2022b).

3.4 Extreme wave events

Investigations on extreme wave events are indispensable for a complete evaluation of a ship. Besides the statistical determination of extreme responses based on investigations in irregular sea state with predefined design wave spectra (and random phase distributions), investigations in deterministic extreme wave sequence enable the deterministic evaluation of critical wave sequences and extreme responses. Particularly, experiments in deterministic extreme wave events allows the detailed analysis of the cause-reaction chain for specific research questions and the evaluation if such wave events are critical for the investigated structure which cannot covered by statistical analysis.

The experiments on extreme wave events comprised investigations based on real world measurements as well as specific design extreme wave groups. As real world reproduction, the famous Draupner wave, also known as "New Year Wave" (Slunyaev et al. 2005; Cherneva and Guedes Soares

(a) VBM at amidships

(b) Wave elevation

(c) Heave motion

(d) Pitch motion
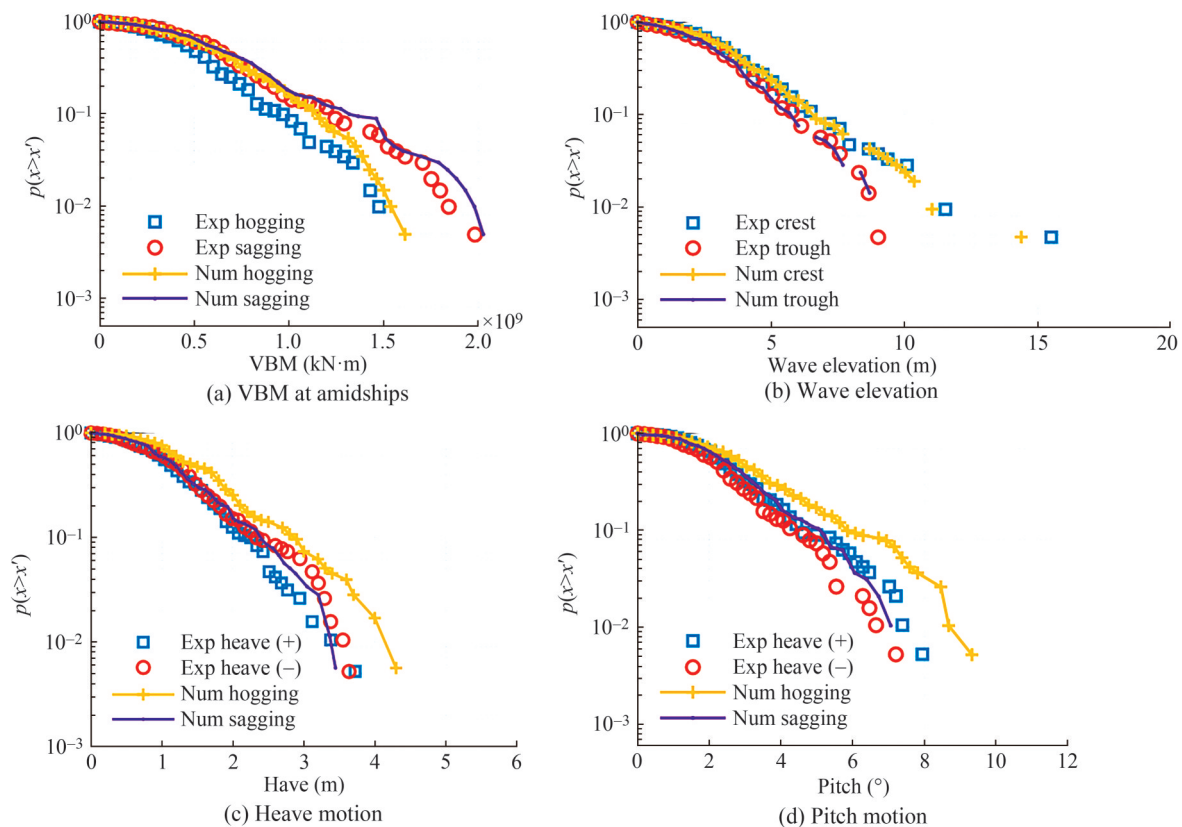
Figure 12   Comparison of the exceedance probability of the peaks for the motions and vbm in sea state IRREGULAR20 phase seed #1
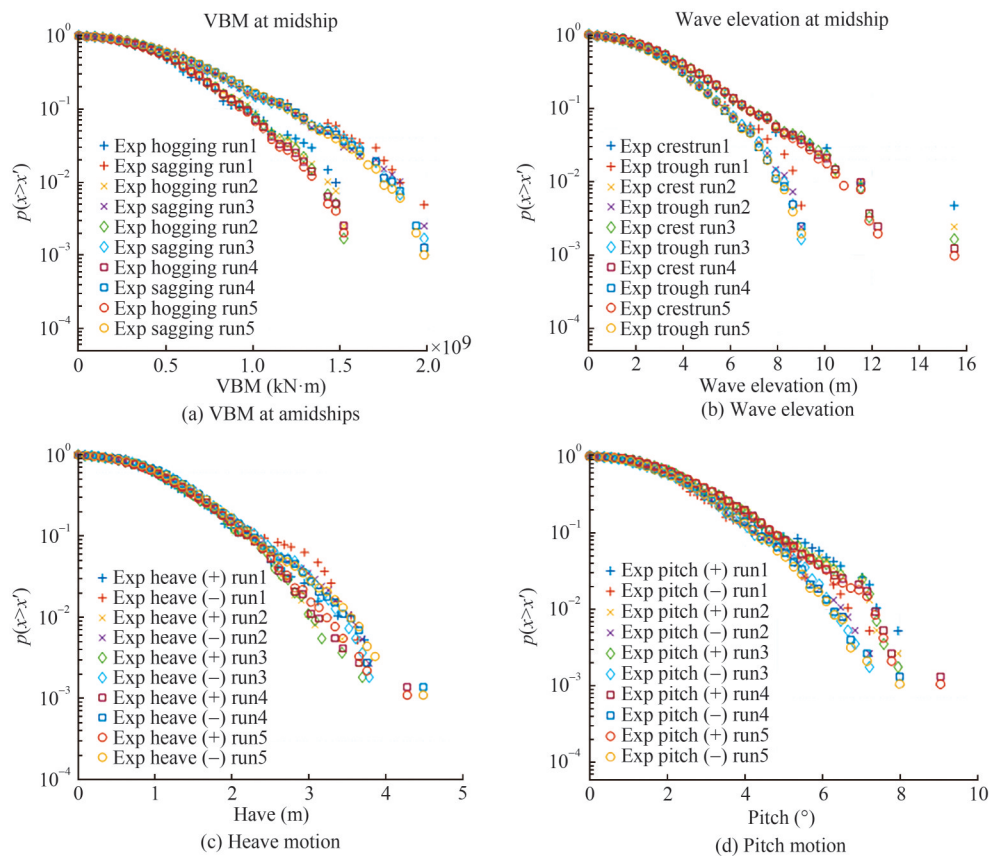
Figure 13 Exceedance probability of peaks for the motions and vbm in sea state IRREGULAR20 all five phase seeds

2008), was generated in the seakeeping basin. Exact solutions of the non-linear Schrödinger (NLS) equation-the so called breather solutions-were applied for the generation of design extreme wave groups. Breather solutions are characterized by quasi-monochromatic waves being slightly perturbed in time or space. Due to modulational instability, this perturbation increases during evolution resulting in large amplifications of the initial amplitude. Altogether, three types of breather solutions, namely the Kusnetzov-Ma breather (Kuznetsov 1977; Ma 1979), the Akhmediev breather (Akhmediev et al. 1985; Akhmediev and Korneev 1986; Akhmediev et al. 1987) and the Peregrine breather (Peregrine 1983), were utilized in order to evaluate their applicability for task related research questions on extreme wave impact.

The application of breather solutions for model tests is beneficial due to several reasons. One aspect relates to the simple and straightforward applicability as design extreme wave: "The major benefits are the potential to generate abnormal waves of certain frequency up to the physically possible wave height, the symmetrical shape of the extreme wave and the availability of an analytical solution" (Klein et al. 2016), which enables a fast and simple generation of the wave maker control signal. Another aspect relates to the fact that breather solutions, particularly the Peregrine breather, are being considered as special prototype of extreme waves (Shrira and Geogjaev 2010). Wang et al. (2018) have shown

numerically that the Peregrine breather is applicable for modeling extreme waves in realistic oceanic conditions by embedding the Peregrine breather in complex sea states based on JONSWAP spectra. In this context, Klein et al. (2016) have shown experimentally that Peregrine breathers can be embedded into irregular sea state to tailored extreme wave sequences and that such a design extreme wave features similar dynamics compared to the real world Draupner wave.

Following, the experiments with the three breather solutions are presented and compared with the results in the Draupner wave. Each solution was used to generate a set of high, steep single waves of different discrete carrier wave lengths to cover the range of interest in frequency domain regarding the vbm. The initial steepness at the wave board were defined in such a way to ensure that the high single wave at target location is as high as physically possible for the defined wave lengths.

3.4.1 Breather-type extreme waves

The three breather solutions applied in the experiments represent exact solutions of the NLS equation which reads

$$\frac{\partial A}{\partial x} + \frac{1}{C_g} \frac{\partial A}{\partial t} + i \left(\alpha' \frac{\partial^2 A}{\partial t^2} + \beta' |A|^2 A \right) = 0 \qquad (1)$$

for the wave group evolution in space of a time series, with
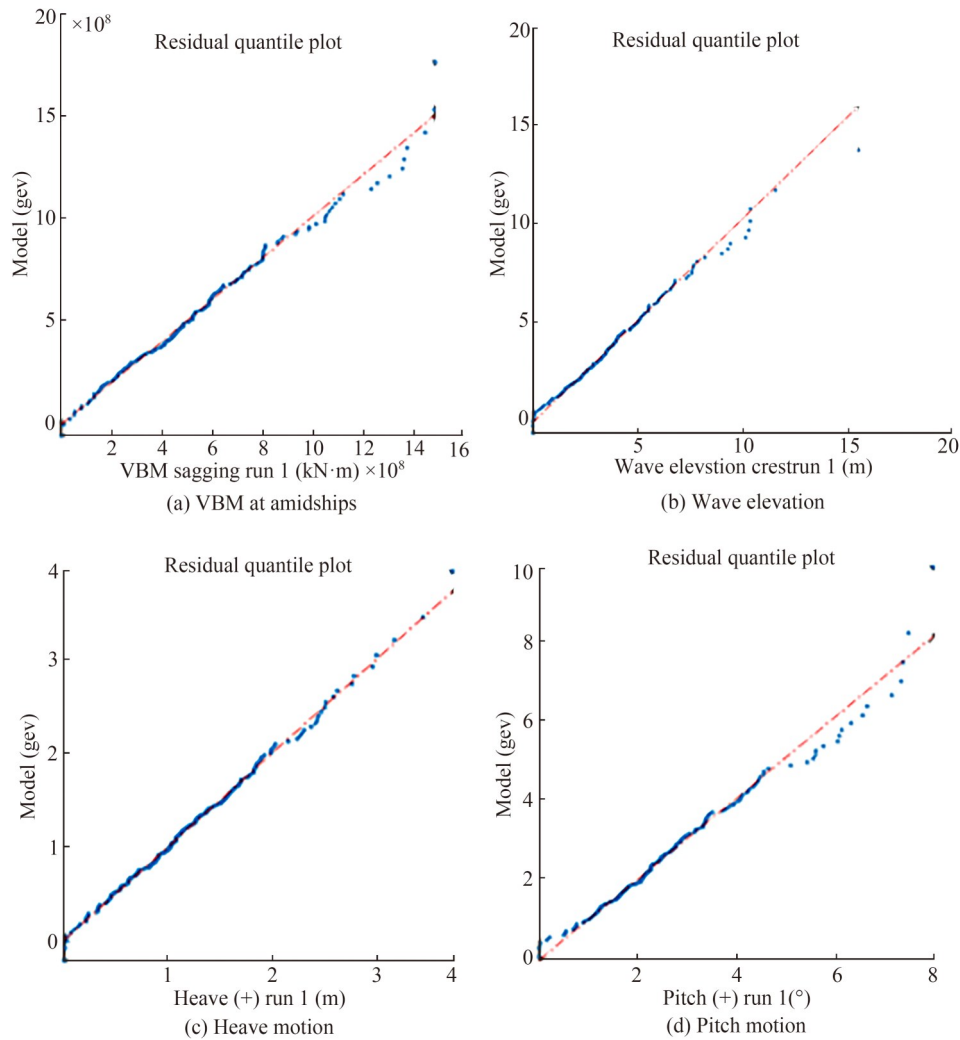
Figure 14   Diagnostic plots of goodness of fit for generalized extreme value (GEV) distribution of the peak values from the experiments

$$\alpha' = \frac{1}{8} \frac{\omega_c}{k_c^{\,2}} \frac{\alpha}{C_g^{\,3}} \tag{2}$$

and

$$\beta' = \frac{1}{2} \omega_c k_c^{\,2} \frac{\beta}{C_g} \tag{3}$$

The coefficients α and β read for arbitrary depth (Serio et al. 2005)

$$\alpha = -v^2 + 2 + 8(k_c d)^2 \frac{\cosh(2k_c d)}{\sinh^2(2k_c d)} \tag{4}$$

$$\beta = \frac{\cosh(4k_c d) + 8 - 2\tanh^2(k_c d)}{8\sinh^4(k_c d)} -$$
$$\frac{(2\cosh^2(k_c d) + 0.5v)^2}{\sinh^2(2k_c d)\left[\dfrac{k_c d}{\tanh(k_c d)} - (\dfrac{v}{2})^2\right]} \tag{5}$$

The carrier wave number is represented by k_c, the corresponding angular frequency by ω_c, the group velocity by C_g and the water depth by d. The correction for the group velocity in finite water depth is taken into account by the coefficient v,

$$v = 1 + 2\frac{k_c d}{\sinh(2k_c d)} \tag{6}$$

3.4.1.1 The Akhmediev breather

The Akhmediev breather (Akhmediev et al. 1985; Akhmediev and Korneev, 1986; Akhmediev et al. 1987) depicts the modulational instability process in space and is periodic in time,

$$A_B(x,t) = A_c(x)\left(\frac{\tilde{v}^2\cosh(\sigma x) - i\tilde{\sigma}\sinh(\sigma x)}{\cosh(\sigma x) - \sqrt{1 - \dfrac{1}{2}\tilde{v}^2}\cos(vt)} - 1\right) \tag{7}$$

with $\tilde{v} = v/a_c \sqrt{\alpha'/\beta'}$, $\tilde{\sigma} = \tilde{v}\sqrt{2 + \tilde{v}^2}$ and $\sigma = \beta'\, a_c^2 \tilde{\sigma}$ (Karjanto and van Groesen 2007). To arrive at the Akhmediev breather solution, three parameters have to be predefined - the plane-wave amplitude a_c, the normalized modulation frequency $\tilde{v}$ as well as the carrier frequency ω_c.

3.4.1.2 The Kusnetzov-Ma breather

The Kusnetzov-Ma breather (Kuznetsov 1977; Ma 1979) is periodic in space and decreases exponentially in time. Contrary to the Akhmediev breather, the modulation for the Kusnetzov-Ma breather is never small, i.e, the solution oscillates while propagating. Consequently, this solution does not comply with the classical Benjamin-Feir instability. The corresponding analytical solution is

$$A_B(x,t) = A_c(x) \left(\frac{-\sqrt{2}\,\tilde{\vartheta}^2 \cos(\eta x) + i\sqrt{2}\,\tilde{\eta}\sin(\eta x)}{\sqrt{2}\cos(\eta x) - \sqrt{2 + \tilde{\vartheta}^2}\cosh(\vartheta t)} - 1 \right) \tag{8}$$

with $\tilde{\vartheta} = \vartheta/a_c \sqrt{\alpha'/\beta'}$, $\tilde{\eta} = \tilde{\vartheta}\sqrt{2 + \tilde{\vartheta}^2}$ and $\eta = \beta'\, a_c^2 \tilde{\eta}$ (Karjanto and van Groesen 2007).

Three parameters have to be predefined in order to determine the breather envelope-the plane-wave amplitude a_c, the normalized modulation wave number $\tilde{\eta}$ as well as the carrier frequency ω_c.

3.4.1.3 The Peregrine breather

The Peregrine breather solution (Peregrine 1983), also known as rational solution, represents the limiting case of the time-periodic Kusnetzov-Ma breather and the space-periodic Akhmediev breather. It has the specific characteristic that it is neither temporally nor spatially periodic: it is a wave that "appears from nowhere and disappears without trace" (Akhmediev et al. 2009) being considered as special prototype of freak wave (Shrira and Geogjaev 2010). Its analytical form suitable for wave tank experiments is (Karjanto and van Groesen 2007)

$$A_B(x,t) = A_c(x) \left(\frac{4\alpha'(1 - i2\beta' a_c^2 x)}{\alpha' + \alpha'(2\beta' a_c^2 x)^2 + 2\beta' a_c^2 t^2} - 1 \right) \tag{9}$$

In general, only the plane-wave amplitude a_c as well as the carrier frequency ω_c (i.e., the initial steepness) needs to be predefined to fully determine the Peregrine solution in space and time.

3.4.1.4 Experimental results

The LNGC was investigated in the three breather solutions introduced above in order to evaluate the applicability of each solution as well as to determine the impact of such high, steep single wave on the LNGC. At the beginning, the three solutions were used to generate a set of high, steep single waves of different discrete carrier wave lengths. The carrier wave lengths were chosen in order to cover the range of interest in frequency domain regarding the vbm-from

L_w/L_{pp}=0.7 to L_w/L_{pp}=1.3. The initial steepness at the wave board was defined in such a way that the high single wave at target location is as high as physically possible for the defined wave lengths.

Based on the different solutions, the determined surface elevation at the wave board was divided by the RAO of the wave maker to obtain the control signal. The agreement between theoretical location of freak wave occurrence (input) and the registrations/observations in the tank showed satisfying agreement, i.e., in most of the cases the actual freak wave event was nearby the given value. But due to the fact that wave-structure investigations implies the definition of target waves in time domain at precise target locations, the investigated breather-type extreme waves presented here resulting from an adjustment of the first control signal to obtain the extreme wave as exact as possible at the target location, i.e., which took up to 3 iteration steps.

Figure 15 presents the results of the model tests at stationary conditions (Fn=0) in breather-type extreme waves-from top, the shortest, to bottom the longest wave length. The LNGC was investigated in three different carrier wave length (L_w/L_{pp}=0.7 to L_w/L_{pp}=1.1) for each of the three breather solutions. In addition, the Peregrine breather was exclusively applied for the L_w/L_{pp}=1.3. The results of each carrier wave length comprises a set of three diagrams-the top diagram shows the surface elevation at the forward perpendicular, the center diagram the vbm at amidships and the bottom diagram the green water column height on deck at the forward perpendicular.

The design vertical wave bending moments according to the IACS-Common Rules (IACS 2015) are additionally illustrated to evaluate the measured vbm, knowing that in the dimensioning process of the transverse section additional parameters have to be considered (e.g., γ_R, c_s, deck openings, ...). The black dashed lines denote the design vertical wave bending moment. The ultimate design vertical wave bending moments, which can be calculated based on design vbm considering safety factors, are not displayed as they are outside the axis scaling (i.e., all data is below this threshold).

The ordinates are equally scaled for all associated diagrams to simplify the overall picture of the results. The different results of the three breather solutions for the same carrier wave length are illustrated in the same set of diagrams-the blue curves denote the results for the Peregrine breather, the red curves for the Akhmediev breather and the green curves the Ma-Kuznetsov breather.

The overall picture of the presented results shows that the high single wave is clearly identifiable at the forward perpendicular-for all breathers and wave length to ship length ratios. Furthermore, it is obvious that the surface elevation of the different breathers with the same carrier wave lengths is quite identical as well as the associated responses, but the Akhmediev breather shows a slightly different wave propagation in front of the target wave. The height of the
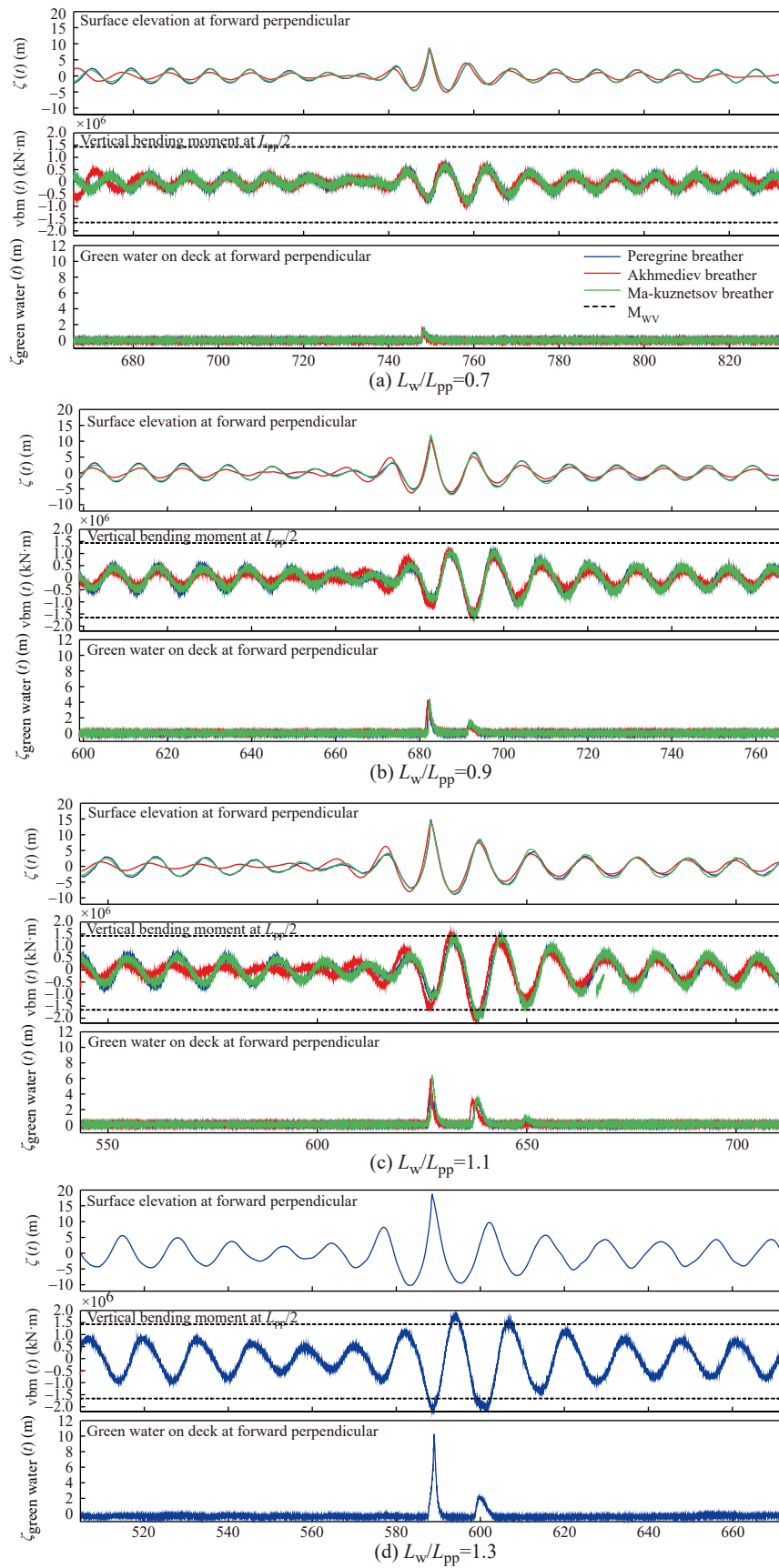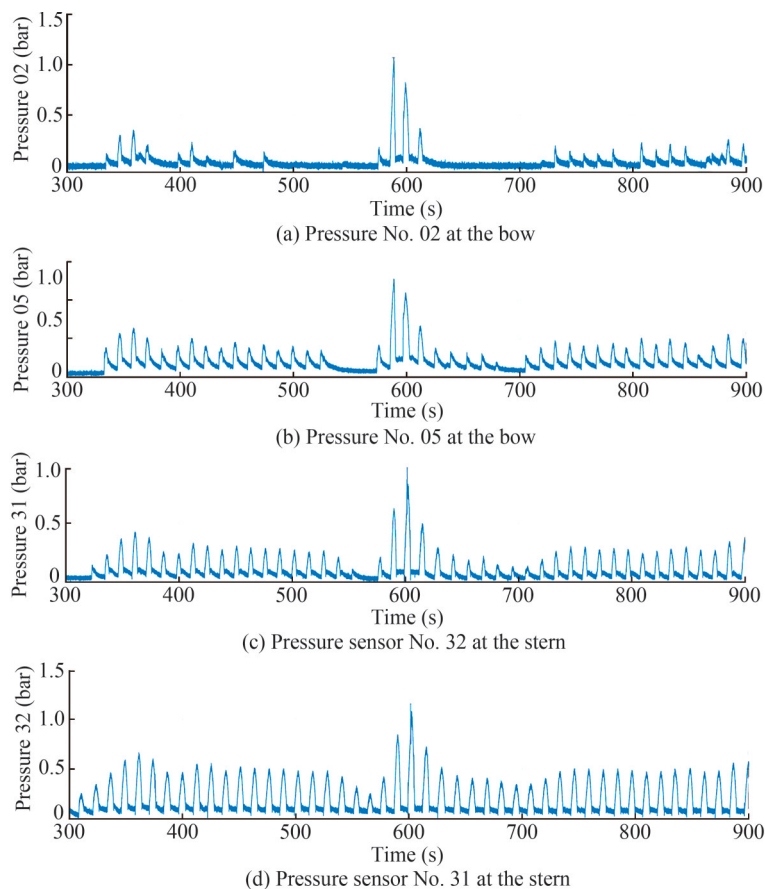
Figure 15   Results of the model tests in breather-type extreme waves

presented extreme waves increases with increasing carrier wave length independently of the used breather solution due to the fact that all presented waves are generated in such a way that the highest physically possible wave height is obtained at the target location, i.e., all presented waves are plunging breaker close to the target location.

Analogue to the results in regular waves, the resulting vbm depends on the wave length and reaches maximum values for the identified critical wave lengths as a function of the wave height. But also the reached absolute values are outstanding due to the impact of the highest physically possible wave height, in contrast to the tests in regular waves with moderate wave steepness. The wave heights of the highest, steepest regular waves (WH3) are approximately 40% smaller compared to the breathers. Comparing the absolute vbm values show that the moments are at least 15% higher for hogging condition and 30% higher for sagging condition than measured in regular waves. The maximum vbm, in particular the sagging moment, reaches the design vertical wave bending moment regarding the LNG Carrier.

The exceeding of the design vertical wave bending moment is not resulting in an inevitable structural failure of the ship at full scale as additional parameters have to be considered for the dimensioning of the transverse section. Nevertheless, it shows that the impact of the breather-type extreme waves is severe and a limiting case for the investigated ship. This is confirmed by the measured green water column heights at the forward perpendicular which reaches impressive values (cf. Figure 10 and Figure 15) - a 10 m high wave front had been detected at the forward perpendicular spilling over the deck which is as high as a single family home. In addition, very high slamming pressure were captured at the bow (pressure sensors No. 02 and No. 05) and stern (pressure sensors No. 31 and No. 32) of the model for the L_w/L_{pp}= 1.3 as seen in Figure 16. For all four recorded pressure sensors, the maximum value occurred when the highest wave impacts the hull. In this Peregrine breather solution, the maximum pressure peaks are 1.07 bar, 1.28 bar, 1.01 bar, and 1.16 bar, respectively. For the L_w/L_{pp}= 1.1 cases, the Peregrine breather solution gives the peaks values as 0.88 bar, 1.00 bar, 0.67 bar, and 0.87 bar, and the Ma-Kuznetsov breather solution provides the peaks as 0.95 bar, 0.99 bar, 0.71 bar, and 0.88 bar, while the Akhmediev breather predicts the peaks as 0.95 bar, 1.18 bar, 0.85 bar, and 1.03 bar. By using the GEV distribution, the most probable extreme values of the peaks on pressure sensors No. 02, No. 05 and No. 32, are 0.82 bar, 0.91 bar and 0.73 bar, for the case in sea state IRREGULAR20 with H_s=11.5 m and T_p=12 s. All the peaks values from the three breather solutions are higher than the extreme values in the irregular

(a) Pressure No. 02 at the bow

(b) Pressure No. 05 at the bow

(c) Pressure sensor No. 32 at the stern

(d) Pressure sensor No. 31 at the stern

Figure 16 Slamming pressure at the bow and stern for Fn=0 in Peregrine Breather extreme wave for L_w/L_{pp}=1.3

case. In particular, the peaks of the the Peregrine breather L_w/L_{pp}= 1.3 case are 31%, 40% and 58% higher than those extreme values.

Altogether, the results show that the breather solutions are a powerful tool for the generation of tailored extreme waves of certain critical wave lengths for investigations of limiting cases on different subjects, e. g., local and global loads, green water effects as well as air gap investigations. In this context, the Peregrine breather solution is particularly advantageous (Klein et al. 2016).

3.4.2 Real world extreme wave reproduction

To evaluate the model test results obtained using the breather solutions, the LNGC was also investigated in a real-world extreme wave reproduction - the famous Draupner wave. The Draupner extreme wave has been recorded during a storm on January 1, 1995 at the Draupner platform in the North Sea. A giant single wave (H_{max}=25.63 m) with a crest height of ζ_c=18.5 m occurred in a surrounding sea state characterised by a significant wave height of H_s= 11.92 m (H_{max}/H_s=2.15). The water depth at the location is d=70 m. Figure 17 shows the measurement in the wave tank in comparison to the original wave sequence recorded at the Draupner platform-see Clauss and Klein (2011) for details on the wave generation procedure.

Figure 18 presents the results for the LNGC at stationary conditions (Fn=0) in the Draupner wave. Figure 18(a) displays the surface elevation at the forward perpendicular, Figure 18(b) the associated vbm and Figure 18(c) the green water on deck at the forward perpendicular. The results obtained in the Draupner wave (blue curves) are compared to the results measured in the Peregrine breather (red curves) with L_w/L_{pp} = 1.3 (cf. Figure 15), respectively. This wave sequence has been chosen due to the fact that the extreme wave at target location features almost the same extraordinarily high wave crest height, but it should be mentioned that the Peregrine breather is also characterized by deeper preceding and following trough as well as shorter up- and downcrossing wave periods, i.e., the Peregrine breather is higher and steeper.

Comparing the measured loads (Figure 18(b)) and green water column on deck (Figure 18(c)) reveals that both extreme waves are dangerous events for the ship. For the Draupner wave impact, the measured vbm reaches the design vertical wave bending moment and the green water column height on deck is with approximately 8 m also impressive. But the impact of the Peregrine breather is more severe resulting in higher hogging and sagging loads as well as green water column height on deck. The main reason for this result is the aforementioned difference between wave height and steepness as well as the wave length of the breather extreme wave as it is more critical regarding the investigated LNGC. This result does not denote that real world registrations reproduced in the wave tank are useless for the evaluation of wave-structure interaction due to the fact that they rep-resent abnormal wave events which happened on sea in contrast to predefined breathers. Therefore, the results obtained in real world freak wave reproductions exclude all possibility of doubt regarding discussions on possible investigated unrealistic, artificial wave sequences. However, this result denotes that the breather solutions can be used to design extreme wave events for certain wave lengths up to the maximum possible wave height for the identification of critical wave sequences regarding wave length, height and steepness.
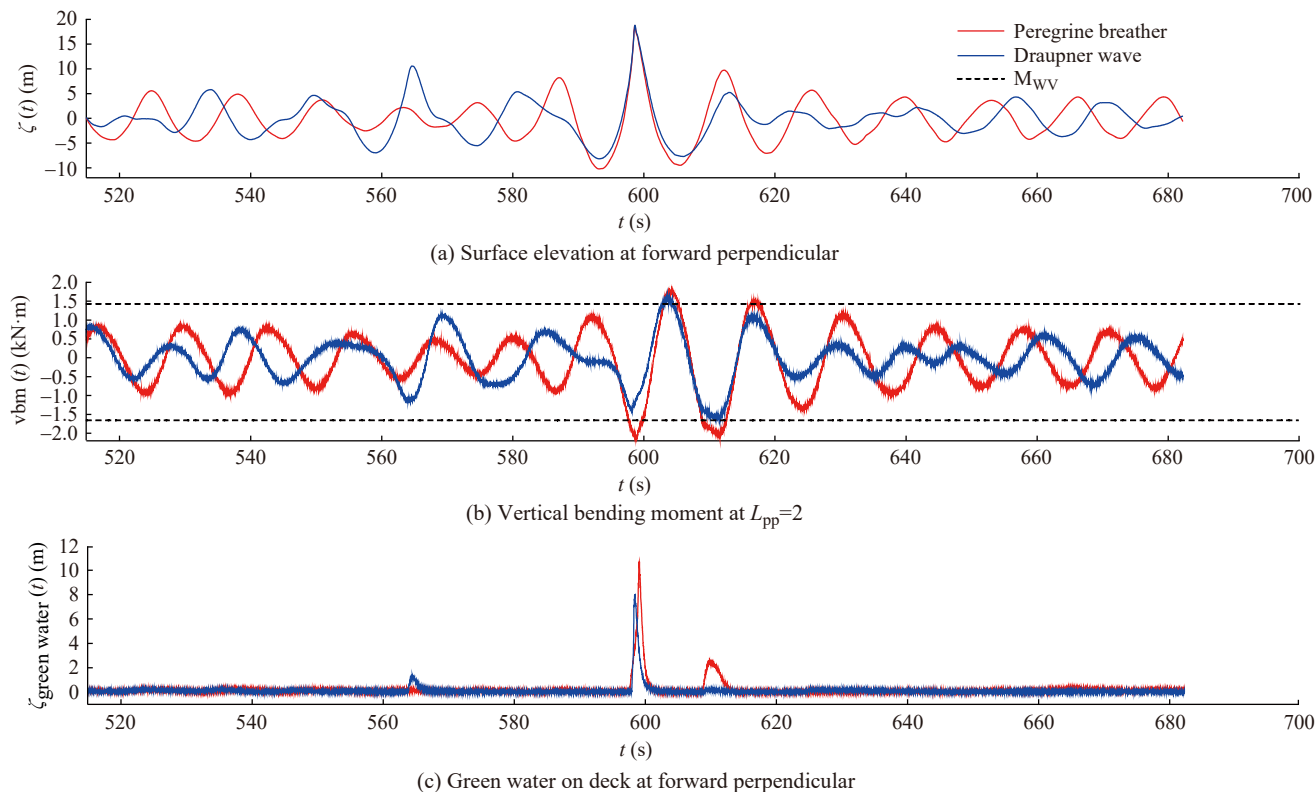
To investigate the impact of the Draupner wave on the motions and loads of the ship, Figure 19 shows the exceedance probability of maxima and minima of the heave and pitch motion as well as the vbm amidships, together with the analytical distribution models by fitting these peaks. It is seen that all the positive peaks are higher than the negative ones for the vbm. The positive peaks are larger than the negative ones at the tails for the distribution of heave and pitch motions. The GEV model fits better on the maxima and minima of the motions, while the Weibull model performs a bit better on the peaks of vbm. By using the GEV model, the most probable extreme values of heave motion are 5.31 m (positive) 6.60 m (negative), and of pitch motion are 7.92° and 7.82°. With the Weibull model, the most probable extreme values of vbm are 1.40×10^9 kN in hogging and 1.63×10^9 kN in sagging. Comparing to the Draupner wave with the Peregrine breather solution (L_w/L_{pp}= 1.3) where the maxima are 4.45 m, 10.41° and 1.78×10^9 kN and minima are 5.43 m, 8.56°, and 2.14×10^9 kN, shows more severity with pitch motion and VBM, although the peaks of the heave motion are 16% (positive) and 18% (negative) lower.

Following, pressure sensors at bow and stern are analyzed calculating the exceedance probabilities of the pressure peaks. For this purpose, three analytical models, Weibull, GEV, and Gumbel distributions, were applied. Figure 20 and Figure 21 show the time series of the measured pressures and the identified peaks for the LNGC for Fn=0 in NYW, on the bow and the stern, respectively. Correspondingly, the exceedance probabilities of the peaks are compared using the three analytical models, Weibull, GEV, and Gumbel distributions. The total number of the identified peaks of sensor 2 is small because it is mounted on the upper part of the flare. When the location is lower (for example, pressure 5), the identified peaks are more. As for the ones at the stern, the total number of the identified peaks is generally larger due to the low draft at the stern. It is observed that the Weibull distribution fits better for the pressure at the bow and the GEV distribution is more suitable for the ones at the stern.

The same analysis was performed by Wang and Guedes Soares (2022a) on the measurements from the case with Fn=0.07, showing the same trends. The extreme values of the pressure peaks obtained using the three distribution models were compared as well. It was found that the ex-
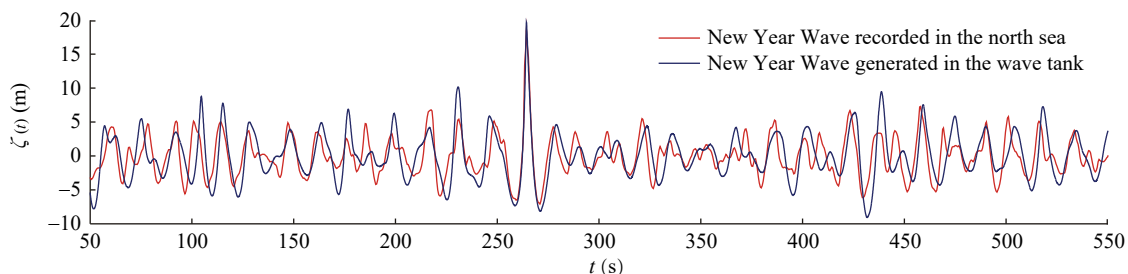
Figure 17 Draupner extreme wave-Comparison of measured model wave train at target position and the recorded sequence at the Draupner platform (full scale)

(a) Surface elevation at forward perpendicular

(b) Vertical bending moment at $L_{pp}=2$

(c) Green water on deck at forward perpendicular

Figure 18 Results of the model tests in the Draupner wave vs. Peregrine breather extreme wave

treme values of the pressure peak were all higher in the case when $Fn=0.07$. The Weibull distribution model provides the highest values, and the Gumbel model predicts the smallest for all the pressures. The differences in the estimation between the three models are in general higher as well when the ship has a forward speed. In general, the extreme pressure is higher at the locations near the calm water surface and is lower at the upper of the flare. Though the total number of the identified pressure peaks on the stern is larger and the geometry of the local structure is flatter, the extreme values there are not higher than the ones on the bow. The maximum peak values of the four pressure sensors are 0.88 bar, 1.03 bar, 0.67 bar, and 0.89 bar. These values are consistent quite well with the ones from the Breather solutions. For example, the ones from the Pere-
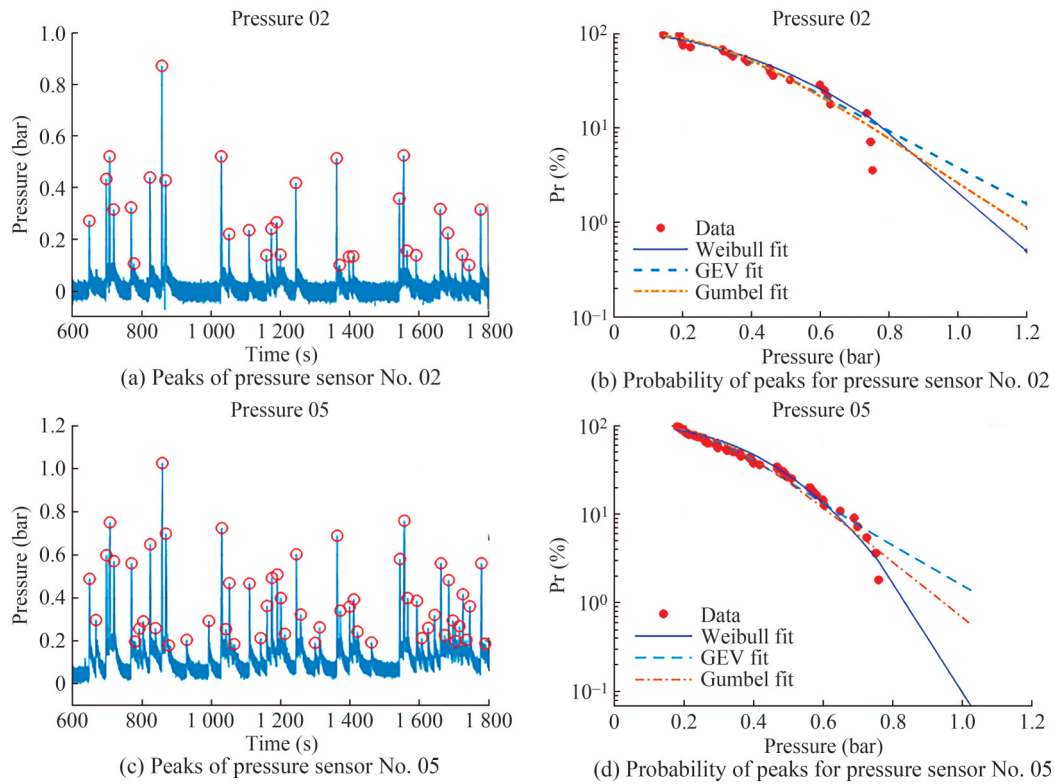
grine breather solution with $L_w/L_{pp}= 1.1$ have around 0.61%, − 2.39%, 0.9% and 2.28% difference relative to the ones from NYW. The results show that the breather solutions are good alternatives to the real work abnormal waves, with regards to the slamming load issue.

4 Conclusion

This paper presented a comprehensive experimental study on the impact of extreme waves on a LNG carrier. It is shown that investigations in the frequency domain, i.e., in transient wave packets and regular waves, are essential to evaluate the overall characteristics in terms of the RAO. In particular the (non-linear) behavior in higher, steeper waves
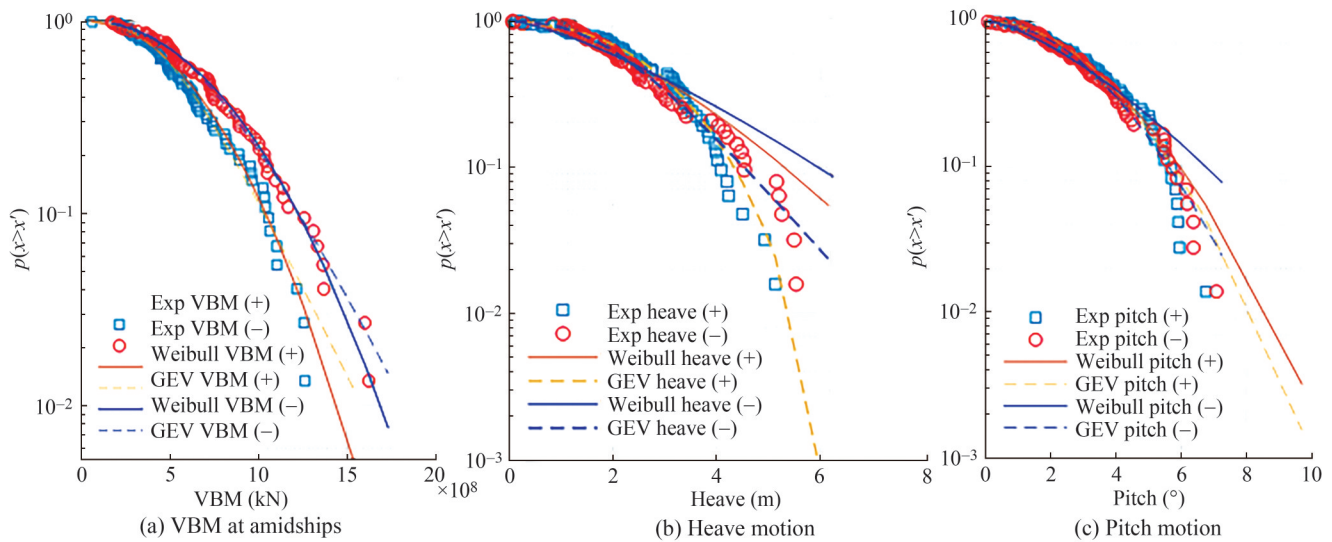
Figure 19 Exceedance probability of peaks for the motions and VBM for the LNGC in the Draupner wave at $Fn=0$

(a) VBM at amidships
(b) Heave motion
(c) Pitch motion

(a) Peaks of pressure sensor No. 02
(b) Probability of peaks for pressure sensor No. 02
(c) Peaks of pressure sensor No. 05
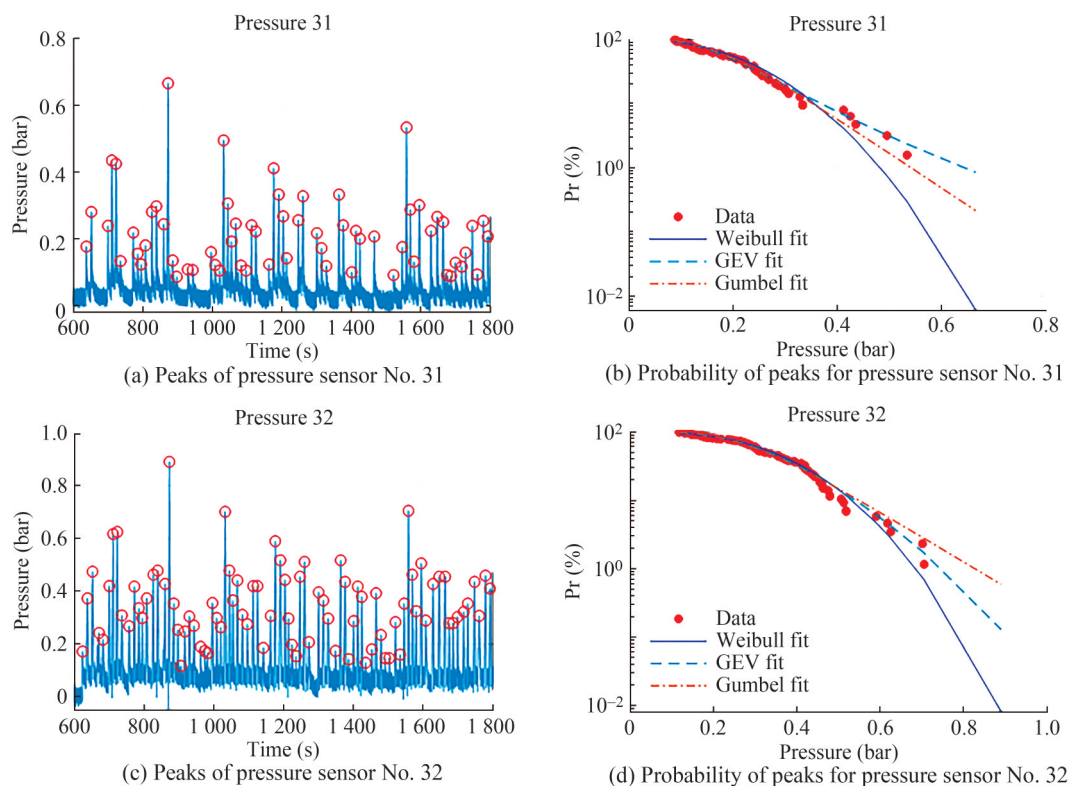(d) Probability of peaks for pressure sensor No. 05

Figure 20 The identified peaks of the pressures at the bow at $Fn=0$ and the corresponding exceedance probability

can be investigated systematically in regular waves. Furthermore, the study revealed that model tests in design extreme waves (i.e., predefined wave length) using breather solutions are a great alternative to search for critical wave sequences in terms of wave length and height. From this it follows that the detected absolute vbm values in breather-type extreme waves are at least 15% higher for hogging condition and 30% higher for sagging condition in comparison to regular

waves of the same wave length. In addition, the impact of the extreme waves resulted in impressive amount of green water on deck.

Investigations in a real world freak wave reproduction-the Draupner wave-showed the same trend: the impact of the extreme wave is severe and dangerous resulting in large loads and huge amount of green water on deck. Evaluating the results in the Draupner wave and in the breather-type

Figure 21   The identified peaks of the pressures at the stern at *Fn*=0 and the corresponding exceedance probability

extreme waves show that larger loads can be observed in the breather-type extreme waves due to the fact that the wave length can be adjusted in order to meet a critical wave length (in contrast to a real world registration). Altogether, this study shows that the breather solutions are a powerful tool for the generation of tailored freak waves of certain critical wave lengths for wave/structure investigations on different subjects, e.g., local and global loads, green water effects as well as air gap investigations and an enrichment for the test portfolio regarding tailored critical wave sequences.

Appendix A Details on ship model mass distribution

Table A1 presents the detailed mass distribution, the corresponding moments of inertia and the center of gravity.

Appendix B Details on pressure transducers

Table B2 presents the positions of the pressure transducers on the hull of the LNGC. The information only provides the *X* and *Z*-coordinates-the corresponding *Y*-position results from the according hull geometry. The positions are given in meters in model scale with the origin located at the aft perpendicular at keel level.

For the model tests, the pressure transducer HKM375-1.7 Bar A from Kulite were installed. The signal amplifiers for the pressure transducers were custom made, designed and manufactured in-house. The motivation for developing in-house signal amplifier lied in the application area. The dynamic pressures were expected to be in a very small measuring range so that only very low-noise amplifier can accurately detect the measured signals. Figure B1 presents time traces of two pressure transducers exemplary. It is shown that the noise level is significantly lower compared to the measured values.

Nevertheless, experimental uncertainties were observed in the model tests, i. e, some of the pressure transducers showed an unusual behavior during the model tests (cf. Figure B1(a)). This can be related to the different temperature compensation behavior of the sensors, even though all sensors should provide the same specifications - a circumstance which has to be taken into account carefully for the interpretation of the measured results. The installed pressure transducers can be classified into three different types

Table A1 Detailed mass distribution, moments of inertia and center of gravity (model scale)
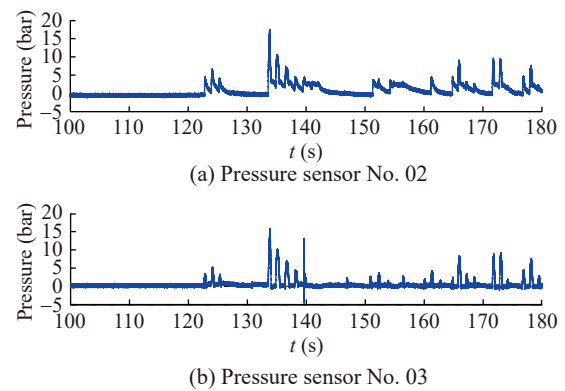
Items	Mass (kg)	Center of gravity			Moment of inertia		
		x (m)	y (m)	z (m)	J_{xx} (kg·m^2)	J_{yy} (kg·m^2)	J_{zz} (kg·m^2)
Fore ship	29.600	1.827	0.000	0.151	0.957	5.283	5.654
Aft ship	24.500	0.784	0.000	0.174	0.917	5.064	4.240
Force transducer	1.800	1.335	0.183	0.283	0.109 2	0.050 0	0.060 7
Force transducer	1.800	1.335	−0.183	0.283	0.109 2	0.050 0	0.060 7
Force transducer	1.800	1.335	0.000	−0.015	0.031 7	0.032 4	0.000 7
Trim weight 1	1.400	2.118	0.000	0.042	0.001 9	0.001 9	0.003 9
Trim weight 2	4.980	2.118	0.000	0.025	0.012 1	0.012 1	0.023 7
Trim weight 3	10.040	1.769	0.000	0.059	0.032 2	0.022 9	0.031 0
Trim weight 4	3.835	1.256	0.074	0.059	0.005 9	0.010 0	0.010 3
Trim weight 5	3.835	1.255	0.074	0.059	0.005 9	0.010 0	0.010 3
Trim weight 6	3.835	1.104	−0.074	0.059	0.005 9	0.010 0	0.010 3
Trim weight 7	3.835	1.103	−0.074	0.059	0.005 9	0.010 0	0.010 3
Trim weight 8	10.040	0.877	0.000	0.059	0.023 0	0.032 1	0.031 0
Trim weight 9	2.020	0.722	0.000	0.019	0.003 0	0.003 0	0.006 1
Trim weight 10	0.340	1.318	0.000	0.308	0.038 1	0.000 1	0.038 1
Trim weight 11	0.057	1.973	0.000	0.311	0.000 0	0.000 0	0.000 0
Trim weight 12	0.057	0.466	0.218	0.501	0.000 0	0.000 0	0.000 0
Trim weight 13	0.057	0.459	−0.218	0.501	0.000 0	0.000 0	0.000 0
Equipped ship model	103.831	1.355	0.000	0.118	2.682	34.811	34.165

Table B2 Positions of the pressure transducers on the LNGC

No.	x (m)	y (m)	No.	x (m)	y (m)	No.	x (m)	y (m)
1	2.730	0.220	2	2.700	0.220	3	2.700	0.195
4	2.670	0.220	5	2.670	0.195	6	2.670	0.170
7	2.640	0.220	8	2.640	0.195	9	2.640	0.170
10	2.640	0.145	11	2.610	0.220	12	2.610	0.195
13	2.610	0.170	14	2.610	0.145	15	2.580	0.220
16	2.580	0.195	17	2.580	0.170	18	2.580	0.145
19	2.550	0.220	20	2.550	0.195	21	2.550	0.170
22	2.550	0.145	23	2.520	0.220	24	2.520	0.195
25	2.520	0.170	26	2.520	0.145	27	2.490	0.220
28	2.490	0.195	29	2.490	0.170	30	2.490	0.145
31	0.000	0.164	32	0.000	0.140	33	0.000	0.125
34	0.030	0.140	35	0.060	0.140	36	2.580	0.000
37	2.700	0.267	38	2.580	0.267			

(a) Pressure sensor No. 02

(b) Pressure sensor No. 03

Figure B1 Time trace of two pressure transducers with normal (B1(b)) and disputable (B1(a)) behavior

of behavior:

• Regular behavior: no shifting pressure offset (cf. Figure B1(b))

• Disputable behavior: a fast shifting offset regarding the reference pressure during each wave impact (cf. Figure B1, top), and a slow decay to the original reference pressure after each wave impact

• Acceptable behavior: a fast shifting offset regarding the reference pressure at the FIRST wave impact, constant offset through the entire test run to be regarded as the new reference pressure level, i.e., no decay to the original reference pressure

Besides systematic uncertainties of some pressure sensors, also the random experimental uncertainties of slamming pressures were estimated (Wang and Guedes Soares 2022b). For this purpose, an irregular sea state with a significant wave height of 11.5 m and a peak period of 12 s described by the JONSWAP spectrum (case IRREGULAR20 in Table C3) was considered. Altogether, five different test runs (different phase seeds) were conducted. Figure B2 presents the time series and the identified peaks for the measurements from two pressure sensors (Figure B2(a) for No. 03 and Figure B2(c) for No. 06-cf. Figure 2(a) and Table B2) in sea state IRREGULAR20 for phase seed #1. Figure B2(b) indicate the goodness of fit for GEV distribution on the selected peaks for pressure sensor No. 03, and Figure B2(d) for pressure sensor No. 06. It was found that
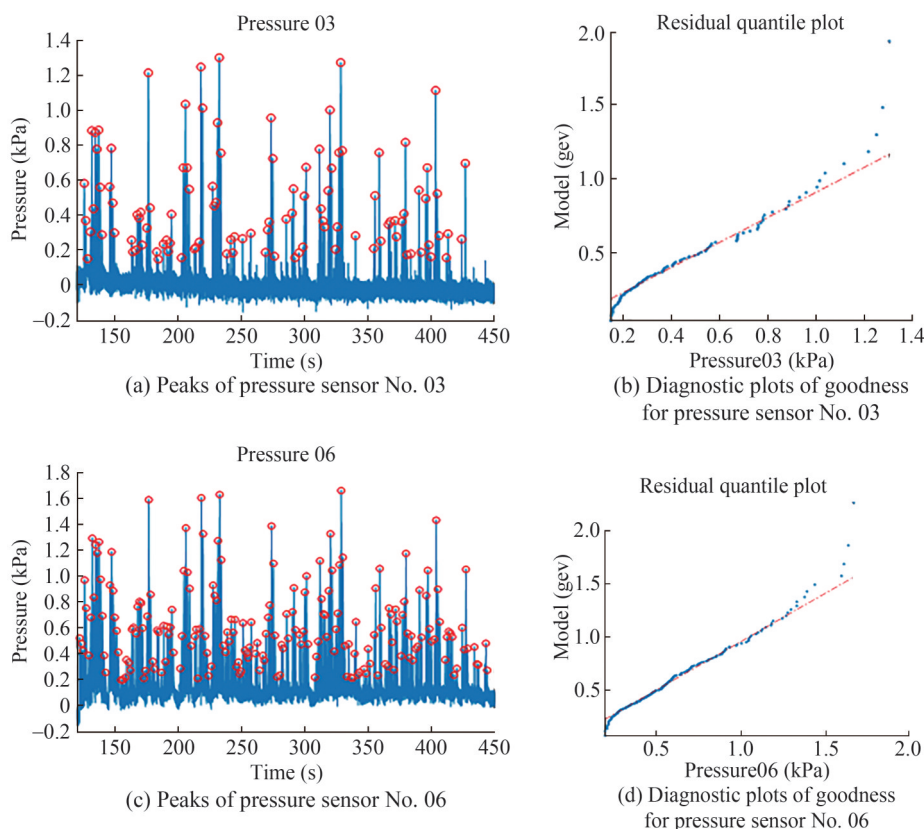
Figure B2 Time series of the pressures and the diagnostic plots of goodness of fit for generalized extreme value distribution of the identified peak values for pressure sensors No. 03 and No. 06

the time series of from phase seed #1 and phase seed #2 were somehow different. The peaks of the pressures from sensors No. 03 and No. 06 are both lower in the measurements from phase seed #2. The extreme value, the average value of the largest 1/10, the average of the largest 1/3 and the mean value of the peaks were calculated, and the random standard uncertainties were calculated as the standard deviation of the metric across the 5 different phase seeds, divided by the square root of the number of observations. The percentages of the relative random uncertainty on the pressure peaks obtained using the data from the five different

phase seeds and the ones excluding phase seed #2 are shown in Figure B3. The uncertainties are much lower when the data from phase seed #2 is excluded.

The study also showed that the GEV distribution model is suitable to study the peak values of the pressures of the hull subjected to extreme waves. The random uncertainties for pressure peaks are slightly higher, eg. 5.94% on the extreme value of pressure sensor 03 for the ship with zero speed (*Fn*=0). However, the values increase greatly for the ship with *Fn*=0.07, e. g., is 11.8% for the same metrics. The complete analysis can be found in Wang and Guedes Soares (2022b).
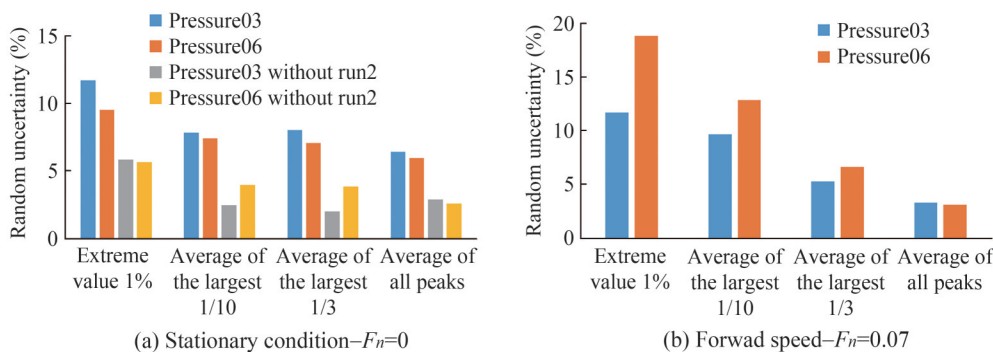
Figure B3 Experimental random uncertainties on the pressure peaks

Appendix C Details on investigated irregular sea states

Table C3   Positions of the pressure transducers on the LNGC

No.	Synonym	H_s (m)	T_p (s)	γ	Phase seeds
1	IRREGULAR13	16.5	16.1	1	5
2	IRREGULAR14	16.5	15.9	3.3	3
3	IRREGULAR15	3	12	3.3	1
4	IRREGULAR16	9.7	12	1	3
5	IRREGULAR17	9.7	12	3.3	5
6	IRREGULAR18	9.7	12	6	5
7	IRREGULAR19	11.5	12	1	3
8	IRREGULAR20	11.5	12	3.3	5
9	IRREGULAR21	11.5	12	6	6
10	IRREGULAR02	8.5	10.92	3.3	1
11	IRREGULAR06	10.5	12.21	3.3	1
12	IRREGULAR10	13.5	13.49	3.3	1
13	IRREGULAR12	16.5	14.78	3.3	1
14	IRREGULAR22	8.5	9.64	3.3	1
15	IRREGULAR23	12.5	12.21	3.3	1
16	IRREGULAR24	13.5	12.21	3.3	1
17	IRREGULAR25	14.5	13.49	3.3	1
18	IRREGULAR$_I$UB	11	11.4	3.3	1

References

Akhmediev N, Ankiewicz A, Taki M (2009) Waves that appear from nowhere and disappear without a trace. Physics Letters A 373(6): 675-678

Akhmediev N, Eleonskii V, Kulagin N (1985) Generation of periodic trains of picosecond pulses in an optical ber: exact solutions. Sov. Phys. JETP 62(5): 894-899

Akhmediev N, Eleonskii V, Kulagin N (1987) Exact first-order solutions of the nonlinear schrödinger equation. Theoretical and Mathematical Physics 72(2): 809-818

Akhmediev N, Korneev V (1986) Modulation instability and periodic solutions of the nonlinear Schrödinger equation. Theoretical and Mathematical Physics 69(2): 1089-1093

Cherneva Z, Guedes Soares C (2008) Non-linearity and non-stationarity of the new year abnormal wave. Applied Ocean Research 30(3): 215-220. https://doi.org/10.1016/j.apor.2008.08.003

Clauss G, Klein M (2011) The new year wave in a seakeeping basin: Generation, propagation, kinematics and dynamics. Ocean Engineering 38(14): 1624-1639. https://doi. org/10.1016/j. oceaneng. 2011.07.022

Clauss G, Klein M (2016) Experimental investigation on the vertical bending moment in extreme sea states for different hulls. Ocean Engineering 119: 181-192. https://doi.org/10.1016/j. oceaneng. 2016. 03.019

Clauss G, Kühnlein W (1995) A new approach to seakeeping Tests of self-propelled models in oblique waves with transient wave packets. Proceedings of the International Conference on Offshore Mechanics and Arctic Engineering, Kopenhagen, Denmark, 279

Clauss G, Kühnlein W (1997) A new tool for seakeeping tests-nonlinear transient wave packets. Proceedings of the 8th Int. Conference on the Behaviour of Offshore Structures (BOSS), Delft, The Netherlands, 269-285

Clauss G, Lehmann E, Östergaard C (1992) Offshore Structures, Volume 1: Conceptual Design and Hydrodynamics. Springer Verlag London

Clauss G, Steinhagen U (1999) Numerical simulation of nonlinear transient waves and its validation by laboratory data. Proceedings of 9th International Offshore and Polar Engineering Conference (ISOPE), Vol. III, Brest, France, 368-375

Clauss GF, Klein M, Dudek M (2010) Influence of the bow shape on loads in high and steep waves. 29th International Conference on Ocean, Offshore and Arctic Engineering: Volume 2, Shanghai, China, 159-170

Clauss GF, Klein M, Dudek M, Onorato M (2012) Application of breather solutions for the investigation of wave/structure interaction in high steep waves. International Conference on Offshore Mechanics and Arctic Engineering, Volume 44892, Rio de Janeiro, Brazil, 123-135

Clauss GF, Schmittner CE, Hennig J, Guedes Soares C, Fonseca N, Pascoal R (2004) Bending moments of an FPSO in rogue waves. International Conference on Offshore Mechanics and Arctic Engineering, Volume 37440, 455-462

Clauss GF, Stuppe S, Dudek M (2014) Transient wave packets: New application in CFD-Methods. Volume 8B: Ocean Engineering of International Conference on Offshore Mechanics and Arctic Engineering, San Francisco, California, USA

Datta R, Guedes Soares C (2020) Analysis of the hydroelastic effect on a container vessel using coupled bem-fem method in the time domain. Ships and Offshore Structures 15(4): 393-402. https://doi.org/10.1080/17445302. 2019.1625848

Denchfield S, Hudson D, Temarel P, Bateman W, Hirdaris S (2009) Evaluation of rogue wave induced loads using 2D hydroelasticity analysis. Proceedings of the 5th International Conference on Hydroelasticity in Marine Technology, University of Southampton, 347-360

Drummen I, Wu M, Moan T (2009) Experimental and numerical study of containership responses in severe head seas. Marine Structures 22(2): 172-193

Fonseca N, Guedes Soares C (1998a) Nonlinear wave-induced responses of ships in irregular seas. Proceedings of the 12th International Conference on Offshore Mechanics and Arctic Engineering, New York, United States. ASME

Fonseca N, Guedes Soares C (1998b) Time-domain analysis of large-amplitude vertical ship motions and wave loads. Journal of Ship Research 42(2): 139-153

Fonseca N, Guedes Soares C (2002) Comparison of numerical and

experimental results of nonlinear wave-induced vertical ship motions and loads. Journal of Marine Science and Technology 6(4): 193-204

Fonseca N, Guedes Soares C (2005) Experimental investigation of the shipping of water on the bow of a containership. Journal of Offshore Mechanics and Arctic Engineering 127(4): 322-330. https://doi.org/10.1115/1.2087527

Fonseca N, Pascoal R, Guedes Soares C, Clauss G, Schmittner C (2010) Numerical and experimental analysis of extreme wave induced vertical bending moments on a FPSO. Applied Ocean Research 32(4): 374-390

Guedes Soares C, Fonseca N, Pascoal R (2008) Abnormal wave-induced load effects in Ship Structures. Journal of Ship Research 52(1): 30-44

Guedes Soares C, Fonseca N, Pascoal R, Clauss GF, Schmittner CE, Hennig J (2006) Analysis of wave induced loads on a FPSO due to abnormal waves. Journal of Offshore Mechanics and Arctic Engineering 128(3): 241-247

Guedes Soares C, Schellin TE (1998) Nonlinear Effects on long-term distributions of wave-induced loads for tankers. Journal of Offshore Mechanics and Arctic Engineering 120(2): 65-70. https://doi.org/10.1115/1.2829525

Guo B, Bitner-Gregersen EM, Sun H, Helmers JB (2013) Prediction of ship response statistics in extreme seas using model test data and numerical simulations based on the rankine panel method. International Conference on Offshore Mechanics and Arctic Engineering, Volume 2A: Structures, Safety and Reliability

Hennig J (2005) Generation and analysis of harsh wave environments. Dissertation Technische Universität Berlin (D 83)

Huang S, Jiao J, Guedes Soares C (2022) Uncertainty analyses on the CFD-FEA co-simulations of ship wave loads and whipping responses. Marine Structures 82: 103129. https://doi.org/10.1016/j.marstruc.2021.103129

IACS (2015) Common structural rules for bulk carriers and tankers. Technical report

Jiao J, Huang S, Tezdogan T, Terziev M, Guedes Soares C (2021a) Slamming and green water loads on a ship sailing in regular waves predicted by a coupled CFD-FEA approach. Ocean Engineering 241: 110107

Jiao J, Huang S, Wang S, Guedes Soares C (2021b) A cfd-fea two-way coupling method for predicting ship wave loads and hydro-elastic responses. Applied Ocean Research 117: 102919

Karjanto N, van Groesen E (2007) Derivation of the NLS breather solutions using displaced phase-amplitude variables. Proceedings of the 5th SEAMS-GMU International Conference on Mathematics and its Applications 2007, Yogyakarta, 357-368

Kharif C, Pelinovsky E, Slunyaev A (2008) Rogue waves in the ocean. Springer Science & Business Media

Klein M, Clauss GF, Rajendran S, Guedes Soares C, Onorato M (2016) Peregrine breathers as design waves for wave-structure interaction. Ocean Engineering 128: 199-212. https://doi.org/10.1016/j.oceaneng.2016.09.042

Klein M, Hartmann M, von Bock und Polach F (2021) Note on the application of transient wave packets for wave-ice interaction experiments. Water 13(12): 1699. https://doi.org/10.3390/w13121699

Kühnlein W, Clauss G, Hennig J (2002) Tailor made freak waves within irregular seas. International Conference on Offshore Mechanics and Arctic Engineering, Volume 36142: 759-768

Kuznetsov E (1977) Solitons in a parametrically unstable plasma. In Akademiia Nauk SSSR Doklady, Vol. 236: 575-577

Lee C (1995) WAMIT theory manual. Technical report, Massachusetts Institute of Technology, Preliminary Copy

Ma Y (1979) The perturbed plane-wave solutions of the cubic schrödinger equation. Studies in Applied Mathematics 60: 43-58

Newman J (2018) Marine hydrodynamics. The MIT Press, Cambridge, Massachusetts

Oberhagemann J, Shigunov V, Moctar O (2012) Application of CFD in long-term extreme value analyses of wave loads. Ship Technology Research 59(3): 4-22

Parunov J, Guedes Soares C, Hirdaris S, Iijima K, Wang X, Brizzolara S, Qiu W, Mikulić A, Wang S, Abdelwahab H (2022) Benchmark study of global linear wave loads on a container ship with forward speed. Marine Structures 84: 103162

Peregrine D (1983) Water waves, nonlinear Schrödinger equations and their solutions. J. Austral. Math. Soc. Ser. B 25(1): 16-43

Rajendran S, Fonseca N, Guedes Soares C (2012) Experiment and time domain method comparison for the responses of a container ship induced by the three sisters abnormal waves. Marine Technology and Engineering, C. Guedes Soares et al. (Ed.), Taylor & Francis, UK: 223-230

Rajendran S, Fonseca N, Guedes Soares C (2015) Simplified body nonlinear time domain calculation of vertical ship motions and wave loads in large amplitude waves. Ocean Engineering 107: 157-177

Rajendran S, Fonseca N, Guedes Soares C (2016) A numerical investigation of the flexible vertical response of an ultra large containership in high seas compared with experiments. Ocean Engineering 122: 293-310

Rajendran S, Fonseca N, Guedes Soares C, Clauss GF, Klein M (2011) Time domain comparison with experiments for ship motions and structural loads on a container ship in abnormal waves. Volume 6: Ocean Engineering of International Conference on Offshore Mechanics and Arctic Engineering, 919-927

Rajendran S, Guedes Soares C (2016) Numerical investigation of the vertical response of a containership in large amplitude waves. Ocean Engineering 123: 440-451

Serio M, Onorato M, Osborne A, Janssen P (2005) On the computation of the benjamin-feir index. Nuovo Cimento della Societa Italiana di Fisica C - Geophysics and Space Physics 28(6): 893-903. https://doi.org/{10.1393/ ncc/i2005-10134-1}

Shrira V, Geogjaev V (2010) What makes the peregrine soliton so special as a prototype of freak waves? Journal of Engineering Mathematics 67(1): 11-22

Simonsen CD, Otzen JF, Joncquez S, Stern F (2013) EFD and CFD for KCS heaving and pitching in regular head waves. Journal of Marine Science and Technology 18(4): 435-459

Slunyaev A, Pelinovsky E, Guedes Soares C (2005) Modeling freak waves from the north sea. Applied Ocean Research 27(1): 12-22. https://doi.org/10.1016/j.apor.2005.04.002

Stansberg C, Karlsen S (2001) Green sea and water impact on FPSO in steep random waves. Practical Design of Ships and Other Floating Structures, Elsevier, 593-601.

Tezdogan T, Demirel YK, Kellett P, Khorasanchi M, Incecik A, Turan O (2015) Full-scale unsteady RANS CFD simulations of ship behaviour and performance in head seas due to slow steaming. Ocean Engineering 97: 186-206

Vassalos D, Guarin L, Jasionowski A, Zheng Y (2003) A risk-based first-principles approach to assessing green seas loading on the hatch covers of bulk carriers in extreme weather conditions. Marine structures 16(8): 659-685

WAMIT (1994) WAMIT Version 5.1-A Radiation-diffraction panel program for wave-body interactions. Technical report, userguide

Wang J, Ma QW, Yan S, Chabchoub A (2018) Breather rogue waves in random seas. Phys. Rev. Appl. 9: 014016. https://doi.org/10.1103/PhysRevApplied.9.014016

Wang S, Guedes Soares C (2016a) Experimental and numerical study

of the slamming load on the bow of a chemical tanker in irregular waves. Ocean Engineering 111: 369-383

Wang S, Guedes Soares C (2016b) Stern slamming of a chemical tanker in irregular head waves. Ocean Engineering 122: 322-332

Wang S, Guedes Soares C (2022a) Analysis of the experimental data of slamming loads on an lng carrier in abnormal waves. Volume 5B: Ocean Engineering; Honoring Symposium for Professor Günther F. Clauss on Hydrodynamics and Ocean Engineering of International Conference on Offshore Mechanics and Arctic Engineering

Wang S, Guedes Soares C (2022b) Random experimental uncertainty analysis on the model tests of an LNG carrier in extreme seas. Volume 5B: Ocean Engineering; Honoring Symposium for Professor Günther F. Clauss on Hydrodynamics and Ocean Engineering of International Conference on Offshore Mechanics and Arctic Engineering

Wang S, Islam H, Guedes Soares C (2021) Uncertainty due to discretization on the ALE algorithm for predicting water slamming loads. Marine Structures 80: 103086. https://doi.org/10.1016/j.marstruc.2021.103086

Wang S, Zhang HD, Guedes Soares C (2016) Slamming occurrence for a chemical tanker advancing in extreme waves modelled with the nonlinear Schrödinger equation. Ocean Engineering 119: 135-142. https://doi.org/10.1016/j.oceaneng.2016.04.017

Wang Y, Wu W, Guedes Soares C (2020) Experimental and numerical study of the hydroelastic response of a river-sea-going container ship. Journal of Marine Science and Engineering 8(12): 978. https://doi.org/10.3390/ jmse8120978

Watanabe I, Ueno M, Sawada H (1989) Effects of bow flare shape to the wave loads of a container ship. Journal of the Society of Naval Architects of Japan 1989(166): 259-266. https://doi. org/ 10.2534/jjasnaoe1968.1989.166-259

Yasukawa H (2002) Application of 3-D time domain panel method to ship seakeeping problems. 24th Symposium on Naval Hydrodynamics, Fukuoka, Japan, 91-106

Zakaria N (2009) Effect of ship size, forward speed and wave direction on relative wave height of container ships in rough seas. Journal of the Institution of Engineers 72(3): 21-34